N-Type Solution-Processed Tin versus Silicon Phthalocyanines: A Comparison of Performance in Organic Thin-Film Transistors and in Organic Photovoltaics

N-type solution-processed tin versus silicon phthalocyanines: comparison of performance in organic thin-film transistors and in organic photovoltaics

Journal:	*ACS Applied Electronic Materials*
Manuscript ID	el-2021-001142.R1
Manuscript Type:	Article
Date Submitted by the Author:	15-Mar-2021
Complete List of Authors:	Cranston, Rosemary; University of Ottawa Faculty of Engineering, Chemical and Biological Engineering Vebber, Mario; University of Ottawa Faculty of Engineering, Chemical and Biological Engineering Rice, Nicole; University of Ottawa Faculty of Engineering, Chemical and Biological Engineering Tonnelé, Claire; Donostia International Physics Center, Castet, Frédéric; Universite de Bordeaux, Institut des Sciences Moléculaires Muccioli, Luca; Universita degli Studi di Bologna, Department of Industrial Chemistry Brusso, Jaclyn; University of Ottawa, Chemistry Lessard, Benoît; University of Ottawa Faculty of Engineering, Chemical and Biological Engineering

N-type solution-processed tin versus silicon phthalocyanines: comparison of performance in organic thin-film transistors and in organic photovoltaics

*Rosemary R. Cranston[†,1], Mário C. Vebber[†,1], Nicole A. Rice[1], Claire Tonnelé[2], Frédéric Castet[3], Luca Muccioli[3,4], Jaclyn L. Brusso[5], and Benoît H. Lessard[1,6,]**

1. University of Ottawa, Department of Chemical and Biological Engineering, 161 Louis Pasteur, Ottawa, ON, Canada
2. Donostia International Physics Center, 4 Paseo Manuel de Lardizabal, 20018 Donostia, Euskadi, Spain
3. Université de Bordeaux, Institut des Sciences Moléculaires, 351 Cours de la Libération, 33405 Talence, France
4. University of Bologna, Department of Industrial Chemistry, 4 Viale Risorgimento, 40136 Bologna, Italy
5. University of Ottawa, Department of Chemistry and Biomolecular Sciences, 150 Louis Pasteur, Ottawa, ON, Canada
6. University of Ottawa, School of Electrical Engineering and Computer Science, 800 King Edward Ave. Ottawa, ON, Canada

[†]Co-first authors

ABSTRACT

Tin (IV) phthalocyanines (SnPcs) are promising candidates for low-cost organic electronic devices, and have been employed in organic photovoltaics (OPVs) and organic thin-film transistors (OTFTs). However, they remain relatively understudied compared to their silicon phthalocyanine (SiPc) analogues. Previously, we reported the first solution processed SnPc semiconductors for OTFTs and OPVs, however the performances of these derivatives was unexpected. Herein to further study the behaviour of these derivatives in OPVs and OTFTs, we report the synthesis along with optical and thermal characterization of seven axially-substituted $(OR)_2$-SnPcs, five of which were synthesized for the first time. Density functional theory (DFT) was used to predict charge carrier mobilities for our materials in their crystal state. The application of these SnPc as ternary additives in poly(3-hexylthiophene) (P3HT)/phenyl-C_{61}-butyric acid methyl ester ($PC_{61}BM$) OPVs and as semiconductors in solution processed n-type OTFTs was also investigated. When employed as ternary additives in OPVs, all $(OR)_2$-SnPcs decreased power conversion efficiency, open-circuit voltage, short circuit current, and fill factor. However, in OTFTs, four of the seven materials exhibited greater electron field-effect mobility with similar threshold voltages compared to their previously studied SiPcs analogues. Among these SnPcs, bis(triisobutylsilyl oxide) SnPc displayed the greatest electron field-effect mobility of 0.014 $cm^2\ V^{-1}\ s^{-1}$, with a threshold voltage of 31.4 V when incorporated into OTFTs. This difference in electrical performance between OTFT and OPV devices was attributed to the low photostability of SnPcs.

Keywords: tin phthalocyanine, silicon phthalocyanine, organic photovoltaics, organic thin-film transistors, photostability, solution processing, N-type organic semiconductor.

INTRODUCTION

Metal and metalloid phthalocyanines (MPcs) are stable and abundant dyes that have been employed as commercial pigments and photoreceptors for over four decades.[1] MPcs also represent a versatile class of semiconductors that exhibit high chemical and thermal stability, large extinction coefficients, and excellent charge carrier mobilities.[2] While MPcs with divalent metal centers such as zinc and copper phthalocyanine (ZnPc and CuPc) have been widely reported as active materials in organic electronic devices,[2,3] MPcs with tetravalent metal centers, such as silicon and tin phthalocyanines (SiPcs and SnPcs), remain relatively unexplored. SiPcs and SnPcs have two axial bonds available for chemical modification, providing additional chemical handles to these materials, and facilitate tuning of their chemical and solid state properties.[1,4–6] SiPcs have recently attracted significant interest as the active material in several emerging applications, such as organic light emitting diodes (OLEDs),[4,7,8] organic photovoltaics (OPVs),[9–12] organic thin-film transistors (OTFTs),[13,14] photopolymerization[15,16] and even photodynamic therapy.[17–19] SnPcs share many of the above listed attractive properties of SiPcs, with the added advantage of more facile and higher-yielding synthesis and purification, as illustrated in **Figure 1**, making them more desirable candidates for low-cost organic electronic devices.[1,4–6,20]

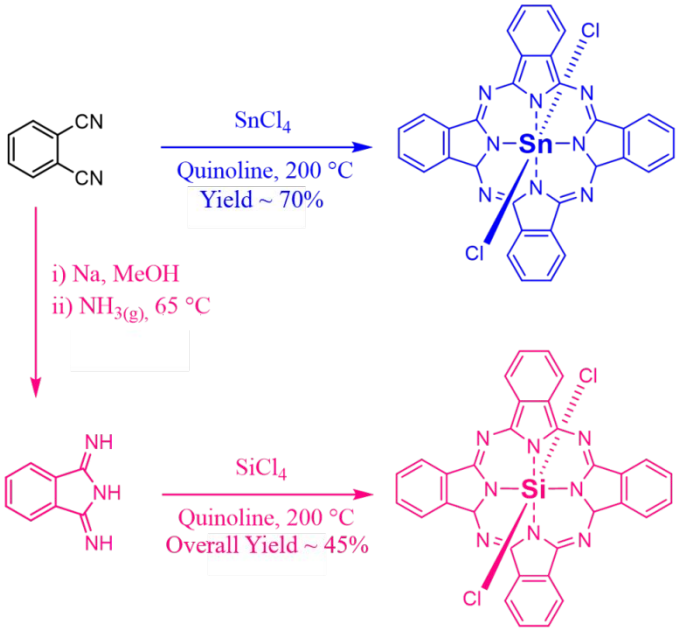

Figure 1. Traditional routes for the synthesis of tetravalent Cl_2-SnPc (blue) and Cl_2-SiPc (pink).

In OPV devices, divalent Sn(II)Pcs have found applications as donors due to their narrow bandgap and p-type conductivity.[21–25] However, there are only a few reports investigating n-type tetravalent Sn(IV)Pcs in OPVs. Two axially-substituted SnPcs ($(OR)_2$-SnPcs) have been employed as ternary additives in poly(3-hexylthiophene) (P3HT) and phenyl-C_{61}-butyric acid methyl ester ($PC_{61}BM$) OPVs.[26] While these two derivatives were able to extend the light absorption range of devices, they led to a reduction in the P3HT/$PC_{61}BM$ contribution to the current density, lowering the overall OPV efficiency. This is in contrast to the performance of OPVs incorporating tetravalent SiPcs, which have been demonstrated to improve device performances and stability.[6,27–30] The authors proposed that the film nano-morphology was the reason for these poor performances; however, more research involving additional derivatives is needed to demonstrate if $(OR)_2$-SnPcs with different axial substituents can circumvent these issues.[26]

OTFTs are critical components for many emerging electronic applications, such as wearable electronics,[31] flexible displays,[32,33] and complementary inverter circuits.[34] Similar to SiPcs, Sn(IV)Pc semiconductors typically exhibit n-type characteristics. Despite their similar structures and less complicated synthesis there are only a few examples of SnPc OTFTs reported in literature, the majority of which were fabricated through vapour deposition of the thin-films from solid materials due to poor solubility.[35–37] Axially-substituted dichloro tin phthalocyanine (Cl_2-SnPc)[36] and tin phthalocyanine oxide (SnOPc)[35] have exhibited electron mobilities (μ_e) of 0.30 $cm^2\ V^{-1}\ s^{-1}$ and 0.44 $cm^2\ V^{-1}\ s^{-1}$, respectively, in vapour deposited OTFTs. To fully realize low-cost OTFTs, solution processable SnPc derivatives are required. Non-conjugated side chains, including substituted alkyl chains, have been extensively demonstrated to improve the solution processability of a variety of polymer[38–40] and small molecule[41–43] semiconductors by increasing solubility while still allowing for close intermolecular packing. To the best of our knowledge, the sole example of solution processed SnPcs are axially-substituted bis(tri-*n*-hexylsilyl oxide) SnPc ($(3HS)_2$-SnPc) and bis(tri-*n*-butylsilyl oxide) SnPc ($(3BS)_2$-SnPc).[26] In this

original study we found that when used as ternary additives in OPVs both $(3HS)_2$-SnPc and $(3BS)_2$-SnPc reduced the overall device efficiency, which we hypothesized was due to their preference for crystallization and phase separation.[26] We recently developed a variety of n-type solution processable $(OR)_2$-SiPcs which were successfully incorporated into both OPV[30] and OTFT[44] devices, and we hypothesize similar functionalization will provide additional insight into the improvement of solution processed SnPcs. More specifically, we found that when matching the solubility of the $(OR)_2$-SiPcs ternary additives with poly(3-hexylthiophene) (P3HT) the most significant in OPV performance enhancement was observed.[30] Therefore, by tuning the solubility of the SnPc derivatives through axial functionalization we should improve its OPV performance enhancement as a ternary additive.

To that end, we herein report the design and synthesis of seven tetravalent SnPcs functionalized with a range of silanes in the axial position (**Figure 2**). Of these derivatives, **SnPc-5** and **SnPc-6** are previously reported,[26] and four of the five novel derivatives were successfully isolated as highly-soluble molecules, with **SnPc-3** degrading during train sublimation. The optical and thermal properties of all seven MPcs were characterized, and crystal structures were obtained for **SnPc-1** (CCDC# 2038511), **SnPc-2** (CCDC# 038512), **SnPc-4** (CCDC# 2038510), **SnPc-5** (CCDC# 1522758)[26], **SnPc-6** (CCDC# 1884805)[26] and **SnPc-7** (CCDC# 2038509). Density functional theory (DFT) was utilized to calculate theoretical HOMO and LUMO energy levels, as well as predict charge carrier mobilities for our $(OR)_2$-SnPc derivatives. The SnPcs were employed as ternary additives in P3HT/PC_{61}BM OPVs and in bottom-gate top-contact (BGTC) OTFTs. Additionally, the photostability of this class of compounds when used in organic electronic device applications was investigated through electrical characterization of OTFTs under illumination. The structural similarities between SnPcs and SiPcs allowed us to directly compare our results with the previously-reported SiPc analogues,[26] allowing us to not only expand the application of tetravalent SnPcs as low-cost n-type semiconductors, but also identify the limitations in relation to other MPc derivatives.

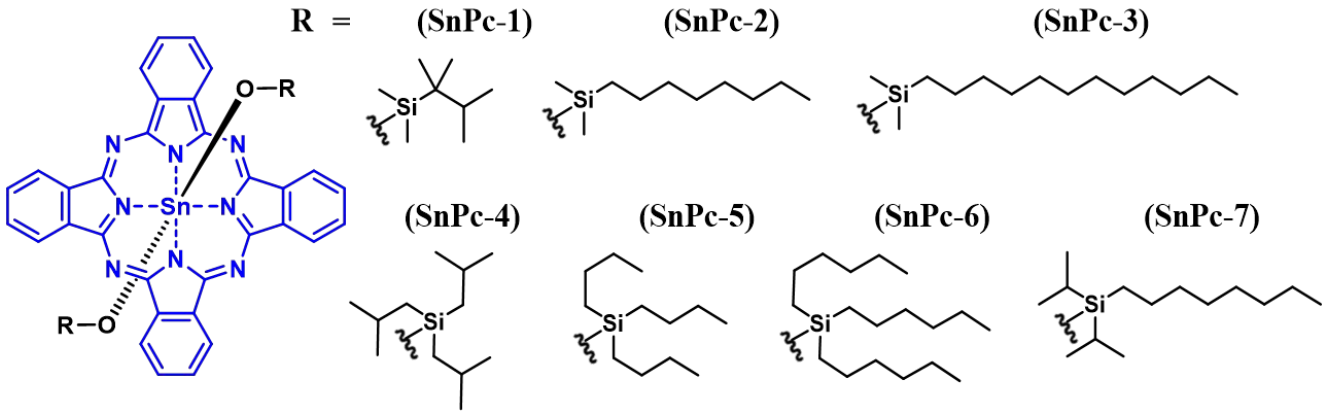

Figure 2. Axially substituted $(OR)_2$-SnPcs synthesized and characterized in the present study.

EXPERIMENTAL SECTION

Materials

Thexyldimethylchlorosilane (>95%), *n*-octyldimethylchlorosilane (>95%), *n*-dodecyldimethylchlorosilane (>95%), tri-*n*-ethylchlorosilane (>95%), tri-*n*-butylchlorosilane (>95%), tri-*n*-hexylchlorosilane (>95%) and *n*-octyldiisopropylchlorosilane (>95%) were purchased from Gelest and used without further purification. Poly(3-hexylthiophene) (MW = 75 kDa, 96% regioregular) was purchased from Rieke Metals and phenyl-C_{61}-butyric acid methyl ester from Nano-C. Solvents were purchased from commercial suppliers and used as received, unless otherwise specified.

Synthesis

Dichloro tin phthalocyanine (Cl_2-SnPc)[45] was synthesized according to literature procedures with minor modifications. Quinoline (10 mL) and phthalonitrile (5.0 g, 39 mmol) were charged into a 100 mL round-bottom flask and purged with nitrogen for 30 min to remove oxygen and moisture. $SnCl_4$ (1.2 mL, 10 mmol) was added to the mixture through a rubber septum and heated at 220˚C for 2 hrs, with constant stirring. The reaction mixture was allowed to cool to 180˚C before the dark-blue powder was isolated by hot filtration and washed with additional quinoline (20 mL), acetone (50 mL) and methanol (100 mL) until the filtrate was clear (67% yield).

The general synthetic procedure for axially-functionalized $(OR)_2$-SnPcs (**Figure 2**) is analogous to the previously reported functionalization of SiPcs.[26] A 50 mL flask was charged with Cl_2-SnPc (1.0 g, 1.4 mmol), chlorobenzene (10 mL), Aliquat HTA-1 (0.015 g, 0.040 ml), trialkylchlorosilane (5.3 mmol), and sodium hydroxide (0.31g, 7.7 mmol) and stirred under reflux (132˚C). A second addition of trialkylchlorosilane (1.68 mmol) was added to the mixture through a rubber septum after 1 h, and the mixture was allowed to reflux for an additional hour. Additional sodium hydroxide (0.12 g, 3.0 mmol) and trialkylchlorosilane (1.68 mmol) were added to the mixture and the reaction was allowed to reflux for an additional 4 hrs before being removed from heat. The dark-teal solution was filtered to remove unreacted solids, and the solvent was removed under reduced pressure. Methanol was added to precipitate the desired product, which was isolated upon filtration by gravity, washed with methanol (70 mL) and dried under reduced pressure. The novel SnPcs were purified via train sublimation (180˚C to 250˚C, 130 mTorr) before their incorporation into OPVs and OTFTs. Reported yields were calculated for the purified product after sublimation, unless otherwise specified.

SnPc-1, Bis(thexyldimethylsilyl oxide) tin phthalocyanine: Yield: 0.51 g (37%). ^{1}H NMR ($CDCl_3$, 400 MHz): δ = 9.62 – 9.68 (m, 8 H), 8.32 – 8.38 (m, 8H), -0.62 – -0.55 (m, 2 H), -1.02 – -0.98 (d, 12 H), -1.26 – -1.24 ppm (s, 12 H), -2.85 – -2.90 ppm (s, 12H). ^{13}C NMR ($CDCl_3$, 100 MHz): δ = 150, 137, 131, 124, 33, 23, 18, 16, -4 ppm. MS (EI): *m/z* calcd for $C_{48}H_{56}N_8O_2Si_2Sn$: 950.29; found: 950.3.

SnPc-2, Bis(*n*-octyldimethylsilyl oxide) tin phthalocyanine: Yield: 0.22 g (15%). ^{1}H NMR ($CDCl_3$, 400 MHz): δ = 9.62 – 9.68 (m, 8 H), 8.32 – 8.38 (m, 8H), 1.12 – 1.27 (m, 4 H), 0.93 – 1.06 (m, 4 H), 0.83 – 0.91 (t, 6H), 0.68 – 0.79 (m, 4H), 0.25 – 0.37 (m, 4H), -0.23 – -0.10 (m, 4H), -1.17 – -1.05 ppm (m, 4H), -2.17 – -2.23 ppm (t, 4H), -2.73 – -2.77 ppm (s, 12H). ^{13}C NMR ($CDCl_3$, 100 MHz): δ = 150, 137, 131, 124, 32 (2), 29, 23, 21, 15, 14, -2 ppm. MS (EI): *m/z* calcd for $C_{52}H_{64}N_8O_2Si_2Sn$: 1006.36; found: 1006.4.

SnPc-3, Bis(*n*-dodecyldimethylsilyl oxide) tin phthalocyanine: Crude quantity: 0.12 g (9%). Crude ^{1}H NMR ($CDCl_3$, 400 MHz): δ = 9.62 – 9.68 (m, 8 H), 8.32 – 8.38 (m, 8H), 0.94 – 1.06 (m, 4 H), 0.79 – 0.94 (m, 26H), 0.66 – 0.78 (m, 4H), 0.25 – 0.36 (m, 4H), -0.23 – -0.11 (m, 4H), -1.17 – -1.03 ppm (m, 4H). Pure compound could not be isolated due to degradation during train sublimation, and therefore was not employed in devices nor further characterized.

SnPc-4, Bis(triisobutylsilyl oxide) tin phthalocyanine: Yield: 0.65 g (43%). ^{1}H NMR ($CDCl_3$, 400 MHz): δ = 9.62 – 9.68 (m, 8 H), 8.32 – 8.38 (m, 8H), -0.62 – -0.55 (d, 36H), -0.81 – -0.71 ppm (m, 6H), -2.28 – -2.32 ppm (d, 12H). ^{13}C NMR ($CDCl_3$, 100 MHz): δ = 150, 137, 131, 124, 26, 24, 22 ppm. MS (EI): *m/z* calcd for $C_{56}H_{72}N_8O_2Si_2Sn$: 1062.42; found: 1062.4.

SnPc-7, Bis(diisopropyloctylsilyl oxide) tin phthalocyanine: Yield: 1 g (62%). ^{1}H NMR ($CDCl_3$, 400 MHz): δ = 9.62 – 9.68 (m, 8 H), 8.32 – 8.38 (m, 8H), 1.21 – 1.33 (m, 4H), 1.04 – 1.16 (m, 4 H), 0.90 – 0.97 (t, 6H), 0.83 – 0.92 (m, 4H), 0.39 – 0.52 (m, 4H), 0.02 – 0.15 (m, 4H), -1.18 – -1.07 (m, 4H), -1.23 – -1.16 (d, 6H), -1.35 – -1.25 (d, 6H), -1.87 – -1.74 ppm (m, 4H), -2.32 – -2.39 ppm (m, 4H). ^{13}C NMR ($CDCl_3$, 100 MHz): δ = 150, 137, 131, 124, 33, 32, 29, 28, 22, 21, 15, 14, 11, 10 ppm. MS (EI): *m/z* calcd for $C_{60}H_{80}N_8O_2Si_2Sn$: 1118.43; found: 1117.5.

Bis(tri-*n*-butylsilyl oxide) tin phthalocyanine (**SnPc-5**) and bis(tri-*n*-hexylsilyl oxide) tin phthalocyanine (**SnPc-6**) were synthesized according to previously reported procedures.[26]

Characterization

Molecular absorption spectroscopy (UV-Vis) spectra of all $(OR)_2$-SnPc compounds were obtained from 0.5 mg mL^{-1} solutions in dichloromethane (DCM), using an OceanView spectrometer, with data collected from 300 – 800 nm. Cyclic voltammetry (CV) and spectropotentiometry (SP) measurements were carried out with a VersaSTAT 3 potentiostat, using a polished platinum disc, an Ag/AgCl electrode and a platinum wire as the working, reference, and counter electrodes, respectively.

For CV analysis, the $(OR)_2$-SnPcs were dissolved in DCM under stirring, tetrabutylammonium permanganate was used as the electrolyte and a scanning rate of 100 mV s^{-1} was applied. The empirical correlation given by E_{HOMO} (eV) = -($E_{ox,onset}$ - $E_{ox\ Fc/Fc+,onset}$) - 4.80 eV was employed to estimate HOMO energy, where $E_{ox,onset}$ and $E_{oxFc/Fc+,onset}$ are the onset oxidation potentials of the sample and of the ferrocene standard, respectively.[46] Thermogravimetric analyses (TGA) were carried out in a nitrogen atmosphere using a TA Instruments Q5000 TGA; samples were heated from 25 – 400˚C at a rate of 5˚C min^{-1}. Degradation temperatures (T_d) were defined by the 5% mass loss cut-off point. Differential scanning calorimetry (DSC) was performed in a TA Instruments Q2000, in three cycles from 0 – 250˚C (or at max 30˚C below the T_d) and at a heating/cooling rate of 5˚C min^{-1}.

Quantum Chemical Calculations

Quantum chemical calculations were performed using the same computational procedures as used in our previous works.[26,44,47] Geometry optimizations and calculations of the molecular energy levels were carried out at the DFT level with the B3LYP exchange-correlation functional, using the Gaussian16 program package.[48] The 6-31G(d) basis set was used for all atoms except Sn, for which the double-ζ-split-valence + polarization (DZVP) basis set was employed.[49] Internal reorganization energies (λ) were calculated at the same level of approximation using the expression derived from the four-point adiabatic potential approach.[50] Electron affinities were obtained as differences between the total energy of the negatively charged and neutral molecules at their respective optimized gas phase geometries. B3LYP/6-31G(d)/DZVP time-dependent (TD) DFT calculations were also carried out to obtain the energies and strengths of the transition toward the two degenerate optically-allowed excited states of isolated molecules.

The electronic couplings (transfer integrals) between nearest-neighbor SnPc pairs in crystal structures were computed using a fragment orbital approach in combination with a basis set orthogonalization procedure.[51] Except for **SnPc-7**, in which significant distortion of the aromatic core is

observed in the crystalline state, the strict degeneracy of the two lowest-unoccupied molecular orbitals (MOs) was assumed for all materials, in line with previous reports.[47] The MOs used for evaluating the transfer integrals were obtained from DFT/B3LYP calculations as implemented in the Orca software,[52] using again the DZVP and 6-31G(d) basis sets for Sn and other atoms, respectively.

Finally, the relative electron mobilities along the crystal axes i = *a, b, c* were evaluated at zero electric field using the following expression in which the energetic disorder in the transport level energies is neglected:

$$\mu_i = \frac{q}{h}\left(\frac{\pi}{k_B T}\right)^{3/2} \frac{1}{\sqrt{\lambda}} \exp\left(-\frac{\lambda}{4k_B T}\right) \sum_k J_k^2 (\vec{r}_k \cdot \vec{e}_i)^2 \quad (1)$$

In **Equation 1**, T = 300 K and the sum runs over all pairs of molecular neighbours separated by the distance vector $\vec{r}_k$ and $\vec{e}_i$ is a cell axis unit vector. Constants q, h and k_B are respectively the elementary charge, the Planck and Boltzmann constants.

OPV Fabrication and Characterization

OPV devices were fabricated on indium-tin oxide (ITO) coated glass (1 in x 1 in) onto which a zinc oxide electron transport layer was deposited by spin-coating a solution of zinc acetate dihydrate (0.196 g) and ethanolamine (0.054 mL) in ethanol (6.0 mL) at 2000 RPM for 1 min. The coated substrate was annealed in air at 180˚C for 1 h, then immediately transferred into a nitrogen glovebox where the remainder of the preparation was carried out. A solution of P3HT (20 mg mL^{-1}), $PC_{61}BM$ (16 mg mL^{-1}) and $(OR)_2$-SiPc (at 3.8%) was spin-coated at 1000 RPM for 35 s to form the active layer, which was allowed to dry at room temperature in a nitrogen environment before being transferred to an evaporation chamber. Electrodes comprised of MoO_3 (7 nm) and silver (70 nm) were deposited through physical vapour deposition (P < 2 x 10^{-6} torr) using an Angstrom EvoVac thermal evaporator to form five individual 0.32 cm^2 OPV devices per substrate, defined by shadow masks.

Current density vs. voltage curves were obtained (in a nitrogen environment) with a Keithley 2400, using a 1000 W m^{-2} AM1.5 xenon lamp for illumination.

OTFT Fabrication

N-doped silicon substrates (15 mm x 20 mm) with a 300 nm thermally grown silicon oxide (SiO_2) dielectric layer were purchased from Ossila. Substrates were cleaned by sequential sonication baths of soapy water, distilled water, acetone and methanol for 5 min each, then dried with nitrogen gas. Substrates were then treated with air plasma for 15 min, before being rinsed with distilled water and isopropanol, and subjected to a surface treatment of 1% v/v octyltrichlorosilane (OTS) in toluene by submersion in solution for 24 hrs at 70˚C. After removal from the OTS solution, substrates were rinsed with toluene and isopropanol and dried in a vacuum oven at 70˚C for 1 h. $(OR)_2$-SnPc solutions were prepared in a nitrogen filled glovebox at a concentration of 10 mg mL^{-1} in chloroform ($CHCl_3$) and heated at 50˚C for 1 h. The solutions were then filtered through 0.2 μm pore size PTFE membranes, and deposited onto the OTS-treated substrates by spin-coating 60 μL of solution at 1500 RPM for 90 s. The films were then either annealed at 100˚C under vacuum for 1 h or left to dry at room temperature in nitrogen. Electrodes were deposited via physical vapour deposition ($P < 2 \times 10^{-6}$ torr) with an Angstrom EvoVac thermal evaporator; electrodes were comprised of 10 nm of manganese and 50 nm of silver, deposited at target rates of 0.5 Å s^{-1} and 1.0 Å s^{-1}, respectively.[13] Shadow masks with a channel width of 1000 μm and length of 30 μm were used, creating twenty individual transistors per substrate. $(OR)_2$-SiPc devices used for testing photochemical stability were fabricated in an identical manner.

OTFT Characterization

Electrical characterization of OTFTs was completed using a custom-built automatic multi-tester, consisting of 48 nickel probe tips plated with 20 nm of gold. The probe tips simultaneously make contact with the source-drain electrodes of the individual transistors, along with the gate electrode. Electrical

characterization was performed on forty individual transistors (across two substrates per $(OR)_2$-SnPc). The multi-tester was kept in a nitrogen filled glovebox for the duration of characterization. The multi-tester introduces an approximate resistance of 750 mΩ to the testing apparatus. A Keithley 2614B and a MCC USB DAQ were used to control the source-drain voltage (V_{SD}) and gate voltage (V_{GS}) to obtain source-drain current (I_{SD}) measurements. The V_{SD} was set constant to 50 V and the V_{GS} varied to obtain I_{SD} measurements in order to determine the saturation regime field-effect mobility (μ_e), threshold voltage (V_T), and on/off current ratio ($I_{on/off}$). **Equation 2** was used to relate μ_e and V_T to V_{GS} and I_{SD} measurements.

$$I_{SD} = \frac{\mu_e C_i W}{2L}(V_{GS} - V_T)^2 \quad (2)$$

Here, W is the channel width (1000 μm), L is the channel length (30 μm), and C_i is the capacitance density. The capacitance density was calculated by the following equation:

$$C_i = \frac{\varepsilon_0 \varepsilon_r}{t} \quad (3)$$

where t is the thickness of the dielectric (300 nm), and ε_r is the relative dielectric constant of SiO_2 (3.9). To determine μ_e and V_T, a linear relationship between I_{SD} and V_{GS} was obtained by taking the square root of **Equation 2** as shown by **Equation 4**.

$$\sqrt{I_{SD}} = \sqrt{\frac{\mu_e C_i W}{2L}}(V_{GS} - V_T) \quad (4)$$

By plotting $\sqrt{I_{SD}}$ versus V_{GS}, μ_e and V_T were determined by the slope and x-intercept, respectively. Lastly, the $I_{on/off}$ is defined as the ratio of the highest and lowest currents measured in the characterized V_{GS} range.

Interfacial Charge Trap Density

The interfacial charge trap density was calculated using the subthreshold swing estimated by the subthreshold region of the characteristic transfer curves of each material. The interface charge trap density (N_i) was calculated by the following equation:[53]

$$N_i = \left(\frac{Sq}{k_B T ln10} - 1\right)\frac{C_i}{q} \quad (5)$$

where S is the subthreshold swing, q is the elemental charge, k_B is the Boltzmann's constant, and T is the temperature.[53,54]

OTFT Photostability Characterization

Photostability characterization of OTFTs were performed in a controlled nitrogen filled glovebox using a Kiethley 2400 under illumination from an AM1.5 solar simulator with a xenon lamp, calibrated with a silicon reference cell (Abet 15150) to 1000 W m^{-2}. OTFTs were sequentially characterized as described above after 15, 30, and 45 min of light exposure, with baseline characterization performed using unexposed devices kept under ambient lighting.

XRD

XRD measurements of thin-films were obtained using a Rigaku Ultima IV powder diffractometer with a Cu Kα (λ = 1.5418 Å) source. Measurements were taken directly from thin-films deposited on silicon substrates with a scan range of $3° < 2\theta < 15°$, and a rate of 0.5° min^{-1} with no spin.

The interplanar spacing (*d*-spacing) between lattice plans was calculated using Bragg's Law shown by the following equation.

$$n\lambda = 2dsin\theta \quad (6)$$

Where λ is the wavelength of the incident wave equal to 1.54056 Å, d is the spacing between planes, θ is the angle of incidence in degrees, and n is a positive integer equal to 1 for this study.

AFM

AFM images were taken using a Bruker Dimension Icon AFM with ScanAsyst-Air tips. ScanAsyst mode was used to collect all images with a scan rate of 1 Hz. NanoScope Analysis v.1.8 software was used for all image processing and editing.

RESULTS AND DISCUSSION

Synthesis and Characterization

The five novel $(OR)_2$-SnPcs (**Figure 2**) were synthesized and their molecular structures characterized as described in the Experimental Section. Overall yields, starting from $SnCl_4$ to final purified materials isolated for incorporation into electronic devices, ranged from 15 – 60 wt%. The only exception was for **SnPc-3**, which could not be successfully purified by train sublimation due to a low degradation temperature, which will be elaborated upon below. The optical, electrochemical and thermal properties of the $(OR)_2$-SnPcs are summarized **Table 1**. All compounds have nearly identical UV-Vis spectra in dichloromethane (DCM) (**Figure S2**) and oxidation potential onsets of approximately 1.12 V, as measured by CV (**Figure S3**). The voltammograms show that the $(OR)_2$-SnPcs have two oxidation events and only one reduction, exhibiting a noticeable difference in the intensities of the opposite redox peaks. Using these results and the empirical correlation E_{HOMO} (eV) = -($E_{ox,onset}$ - $E_{ox\ Fc/Fc+,onset}$) - 4.80 eV,[46] the HOMO and LUMO levels of the $(OR)_2$-SnPcs have all been estimated to be around -5.5 and -3.7 eV, respectively, consistent with previously reported measurements,[26] which is further evidence that the changes in length of the axial groups have a minimal effect on the bandgap (E_g) and electron affinity of $(OR)_2$-SnPcs. Additionally, the acquired voltammograms varied significantly after each cycle, indicating irreversible oxidation. While behavior has been described for unsubstituted SnPcs, where both anionic and cationic forms of the SnPc where observed after redox processes,[55] it is in contrast to SiPcs, which have not been reported to undergo irreversible degradation at similar redox potentials.[30]

The thermal properties of the $(OR)_2$-SnPcs were assessed using both TGA and DSC techniques (**Figure S4, Figure S5** and **Table 1**). While the degradation temperature (T_d) of $(OR)_2$-SiPcs has been reported to be in the range of 300 – 400˚C,[6,30] the T_d of most of our $(OR)_2$-SnPc derivatives are much lower, between 200 – 350˚C. The only exception is **SnPc-3**, which degrades at 194˚C and therefore could

not be purified by train sublimation; hence was not characterized further or incorporated into electrical devices. **SnPc-2** had the second lowest measured T_d of 213˚C and produced the lowest yield (15%), suggesting that the low yield might be related to its thermal sensitivity. Given the high thermal stability of the phthalocyanine ring (stable up to 400˚C),[56] it is likely that the Sn-O bond in the metal center is not as stable at high temperatures as the Si-O bond present in $(OR)_2$-SiPcs. Moreover, it can be noticed that $(OR)_2$-SnPcs substituted with branched silanes have higher thermal stability than their unbranched counterparts with identical MW (**SnPc-3** compared to **SnPc-7**, and **SnPc-4** compared to **SnPc-5**). In **Figure S5**, **SnPc-7** was the only material to display a thermal event in the analysed DSC range: a hysteretic transition between 138˚C (cooling) and 167˚C (heating). The hysteresis could indicate liquid crystalline behaviour, however, more experiments are needed to confirm this hypothesis as it could also be simply an artifact due to supercooling.

Table 1. Synthetic yields, optical, electrochemical and thermal characterization, as well as solubility in dichlorobenzene of the $(OR)_2$-SnPcs.

Material	*Yield* (%)	λ_{max}[a] (nm)	E_g[a] (eV)	E_{Ox}[b] (eV)	E_{HOMO}[c] (eV)	E_{LUMO}[c] (eV)	T_d (˚C)[d]	Solubility (mg mL^{-1})[e]
SnPc-1	37	683	1.77	1.11	-5.50	-3.73	348	12
SnPc-2	15	683	1.77	1.11	-5.50	-3.73	213	117
SnPc-3	9	-	-	-	-	-	194	-
SnPc-4	43	683	1.77	1.10	-5.49	-3.72	305	69
SnPc-5[f]	52	682	1.78	1.13	-5.52	-3.74	227	40
SnPc-6[f]	58	682	1.78	1.13	-5.52	-3.74	199	72
SnPc-7	63	682	1.78	1.12	-5.51	-3.73	241	248

a. absorbance peak measured in DCM solution; E_g = is the energy bandgap calculated from the peak onset
b. half wave potential of oxidation measured using an Ag/AgCl reference electrode and platinum rod working electrode in DCM solutions
c. E_{HOMO} = is the HOMO energy level estimated using the empirical correlation E_{HOMO} (eV) = -($E_{ox,onset}$ - $E_{ox\ Fc/Fc+,onset}$) - 4.80. LUMO energy levels were determined from $E_{LUMO} = E_{HOMO} + E_g$.
d. degradation temperature defined as a 5% reduction in the sample mass
e. measured by filtering a saturated solution of the $(OR)_2$-SnPc in dichlorobenzene and weighing solid content after solvent evaporation.
f. data from ref 26

Quantum Chemical Calculations

Table 2 reports the electronic and absorption properties of individual molecules, as computed in the gas phase at the DFT level. Consistent with CV measurements, energy bandgaps and electron affinities weakly depend on the chemical nature of the axial groups. As shown previously for **SnPc-5** and **SnPc-6**,[26] SnPc derivatives display HOMO and LUMO levels ~ 0.2 eV deeper than their $(OR)_2$-SiPc analogs, without significant change on the energy bandgaps. On the other hand, electron affinities of $(OR)_2$-SnPc derivatives are larger by 0.3 eV than for $(OR)_2$-SiPcs. Except for **SnPc-5** and **SnPc-6**, SnPcs also exhibit slightly larger reorganization energies, which is expected to weaken the electron hopping rates and thus to be detrimental for charge transport.

Since the nature of the axial substituent hardly affects the frontier energy levels, all compounds display similar $S_0 \rightarrow S_1$ transition energies ($\Delta E_{01} \sim 2$ eV) and oscillator strength ($f_{01} \sim 0.35$). DFT calculations also predict that the first absorption band in $(OR)_2$-SnPc derivatives is slightly red-shifted (by ~ 0.03 eV) compared to $(OR)_2$-SiPc ones.[44] The small impact on the absorption properties of the nature of the axial groups and of the metal/metalloid center is consistent with the fact that the frontier molecular orbitals involved in the two degenerate low-lying transitions are spread only over the phthalocyanine backbone, with no delocalization on core and axial substituents, as confirmed also by the electrochemical gaps reported in **Table 1** and by the experimental absorption spectra shown in **Figure S2**.

Table 2. DFT energy values of the HOMO, LUMO, LUMO+1, electron affinity (EA, obtained from differences in the total energies of the charged and neutral molecules in their optimized geometries), internal reorganization energies (λ) and TD-DFT vertical transition energies (ΔE_{01} and ΔE_{02}) and oscillator strengths (f_{01} and f_{02}) from the ground state (S_0) towards the nearly-degenerate excited singlet states (S_1 and S_2), calculated at the B3LYP/6-31G(d) level. All energy values are given in eV.

Material	E_{HOMO}	E_{LUMO}	E_{LUMO+1}	EA	ΔE_{01} (f_{01})	ΔE_{02} (f_{02})	λ
SnPc-1	-5.34	-3.19	-3.19	2.27	2.03 (0.352)	2.04 (0.350)	0.231
SnPc-2	-5.32	-3.17	-3.17	2.26	2.04 (0.361)	2.04 (0.358)	0.270
SnPc-4	-5.37	-3.23	-3.22	2.32	2.02 (0.337)	2.03 (0.336)	0.236
SnPc-5[a]	-5.37	-3.23	-3.22	2.34	2.02 (0.349)	2.03 (0.339)	0.234
SnPc-6[a]	-5.39	-3.26	-3.24	2.39	2.01 (0.359)	2.03 (0.338)	0.259
SnPc-7	-5.35	-3.20	-3.20	2.30	2.03 (0.347)	2.03 (0.347)	0.246

a. data from ref 26

Transfer integrals characterizing the electronic coupling between molecular neighbours in crystal structures can be found in **Table S1**. Crystals were grown by slow evaporation of $(OR)_2$-SnPcs solutions in DCM. Note that single crystals were obtained only for **SnPc-1, SnPc-4**, **SnPc-5**, **SnPc-6** and **SnPc-7**. As discussed above, **SnPc-3** decomposed during sublimation and could not be purified, while only a solvated crystal was obtained for **SnPc-2**. In the case of **SnPc-4**, two different crystal structures were obtained (labelled **SnPc-4a** and **SnPc-4b** in **Table S1**). Single crystal XRD and XRD patterns of thin-films suggest that both crystal structures of **SnPc-4** are present in OTFT devices using the fabrication conditions of this study (**Figure S6**), given by the peak located at approximately $2\theta = 8.5^\circ$ with Miller indices of (0,1,-1). It is also worth stressing that charge-transport properties calculated for defect-free single crystals or for polycrystalline structures cannot be directly compared to experimental measurements performed on amorphous thin-films, in which charge carrier mobilities are impacted by spatial and energetic disorder induced by inhomogeneities, surface roughness or grain boundaries.[57–59] However, mobilities computed based on single crystal supramolecular arrangements may be considered as the maximum that is achievable for the intrinsic defect-free material, and thus as an upper limit to

experimentally measured mobilities, which are typically two orders of magnitude lower than single crystal ones in the case of polycrystalline thin-films.

When calculated at the molecular geometries obtained from X-ray measurements, the LUMO and LUMO+1 are nearly degenerate (with energy differences all below 0.1 eV), with the notable exception of **SnPc-7,** for which the energy difference between the two MOs amounts to 0.6 eV. This important lifting of degeneracy originates from a significant geometrical distortion of the phthalocyanine backbone, evidenced by a much larger alternation in the C-N bond lengths as compared to the other materials (**Figure S7**). In all other compounds, the contribution of the two lowest vacant MOs largely strengthens the hopping rates between adjacent molecular sites, by offering two possible electronic couplings instead of a single one.

Contrary to single molecule properties, transfer integrals strongly depend on the nature of peripheral substituents, since the latter are responsible for the relative positioning of neighboring molecules in the crystals. Within the $(OR)_2$-SnPc series reported herein, **SnPc-2** displays the largest electronic couplings (J_k = 64 and 47 meV along the (1/2, 0, 1/2) and (-1/2, 0, 1/2) directions, respectively), which are expected to give rise to efficient electron-conducting channels. The main coupling terms in **SnPc-5** and **SnPc-6** are two times lower (32 and 29 meV along the ± (1, 0, 0) and (1/2, 0,-1/2) directions, respectively), while **SnPc-1**, **SnPc-4** and **SnPc-7** exhibit the lowest coupling terms within the series.

The large variations in the intermolecular couplings from one system to another strongly influence the magnitude and dimensionality of electron mobilities (**Table 3**). **SnPc-2** displays the largest computed average mobility (μ_{avg} = 1.1 $cm^2\ V^{-1}\ s^{-1}$), as well as nearly 3D charge transport properties in the crystalline phase, two features which in principle make it a promising candidate for the realization of high-performing organic semiconductors. Indeed, materials with multidimensional conductivity are prone to achieve charge transport over long distances, since the availability of multiple pathways makes those materials less sensitive to spatial defects. Crystal **SnPc-5** has a mobility about 2.4 times smaller

than **SnPc-2**, but with a pronounced 2D character. **SnPc-6** and **SnPc-7** display similar average mobilities ($\mu_e \sim 0.2$ cm^2 V^{-1} s^{-1}) but with different charge transport dimensionalities. Finally, **SnPc-1** and **SnPc-4** present the lowest electron mobilities within the SnPc series. Noteworthy, with the exception of these last two compounds, $(OR)_2$-SnPcs display larger mobilities than their $(OR)_2$-SiPc analogues.[44]

Table 3. Computed electron mobilities along *a, b, c* crystallographic directions (with maximum values in bold), average mobility ($\mu_{avg} = (\mu_a + \mu_b + \mu_c) / 3$), and dimensionality ($D$) of the electron transport (as defined in ref 47)

Material	μ_a (cm^2 V^{-1} s^{-1})	μ_b (cm^2 V^{-1} s^{-1})	μ_c (cm^2 V^{-1} s^{-1})	μ_{avg} (cm^2 V^{-1} s^{-1})	D
SnPc-1	0.011	0.098	**0.108**	0.072	2D
SnPc-2	0.651	0.329	**2.329**	1.103	2D
SnPc-4a	**0.146**	0.119	0.000	0.088	2D
SnPc-4b	0.018	**0.095**	0.061	0.058	2D
SnPc-5[a]	**1.099**	0.296	0.003	0.466	1D
SnPc-6[a]	0.270	0.071	**0.307**	0.216	2D
SnPc-7	**0.482**	0.127	0.020	0.210	1D

a. data from ref 26

Device Performance

Ternary organic photovoltaics (OPVs)

The six successfully synthesized $(OR)_2$-SnPcs were incorporated into P3HT/PC_{61}BM OPV devices at 3.7% concentration, which parallels previous experiments adding $(OR)_2$-SiPc to P3HT/PC_{61}BM ternary BHJ OPV devices,[26] allowing a direct comparison of the performance between the two families of phthalocyanines. The HOMO/LUMO levels of the $(OR)_2$-SnPcs are in between those of P3HT and PC_{61}BM, and therefore should be well suited for ternary additive applications. However, as shown in **Table 4**, incorporation of all $(OR)_2$-SnPcs resulted in a moderate decrease in overall device performance, a substantially different result compared to previously reported $(OR)_2$-SiPcs,[30] which were shown to greatly improve current and power conversion efficiency (*PCE*) in almost all cases. An illustrative comparison is shown in **Figure 3** between the P3HT/PC_{61}BM baseline device, a ternary

device made using **SnPc-6**, and the analogous ternary device made with **SiPc-6** derivative (published in a previous report),[30] both at the same additive concentration of 3.7%. Clearly the addition of **SiPc-6** improves device performance while the addition of the **SnPc-6** hinders it. Furthermore, EQE curves (**Figure 3c**) show that, while $(OR)_2$-SnPc additives extend the absorption range beyond 700 nm, the intensity of the P3HT/$PC_{61}BM$ contribution (350 – 600 nm) is reduced, which is not observed with the addition of $(OR)_2$-SiPcs. The structure, solubility and optoelectronic properties of both classes of $(OR)_2$-SnPc and $(OR)_2$-SiPcs[30] are very similar and therefore does not explain the disparity in their effectiveness as ternary additives. In previous work,[26] where only **SnPc-5** and **SnPc-6** were assessed, the addition of $(OR)_2$-SnPc additives also led to a decrease in device performance, which was hypothesized to be a result of poor film morphology. However, this persistent device performance hindrance observed for all $(OR)_2$-SnPc derivatives, combined with the demonstrated irreversible redox processes in the CV analysis, discredits our previous hypothesis, and points to a fundamental instability of $(OR)_2$-SnPc when involved in redox reactions, which will be elaborated upon below.

Table 4. Current density - voltage results for all assembled OPVs, including *PCE*, open circuit voltage (V_{OC}), short circuit current (J_{SC}) and fill factor (*FF*).

Device[a]	*PCE*[b] (%)	*Voc*[b] (V)	*Jsc*[b] (mA cm^{-2})	*FF*[b]
Baseline	2.78± 0.11	0.52 ± 0.01	9.59± 0.37	0.56 ± 0.01
SnPc-1	1.17 ± 0.21	0.45 ± 0.01	6.47 ± 1.00	0.40 ± 0.00
SnPc-2	1.14 ± 0.07	0.41 ± 0.01	7.03 ± 0.35	0.40 ± 0.00
SnPc-4	1.94 ± 0.09	0.46 ± 0.00	9.22 ± 0.22	0.46 ± 0.01
SnPc-5	2.01 ± 0.03	0.47 ± 0.01	8.85 ± 0.09	0.48 ± 0.00
SnPc-6	2.04 ± 0.07	0.48 ± 0.00	9.20 ± 0.16	0.47 ± 0.00
SnPc-7	1.90 ± 0.05	0.46 ± 0.00	8.84 ± 0.21	0.46 ± 0.00

a. active layer composed of P3HT:PCBM:$(OR)_2$-SnPc (3.78%), spin-coated at 1000 RPM, dried in nitrogen, no annealing
b. values calculated from I-V curves, average of five devices, 1000 W m^{-2} irradiation power

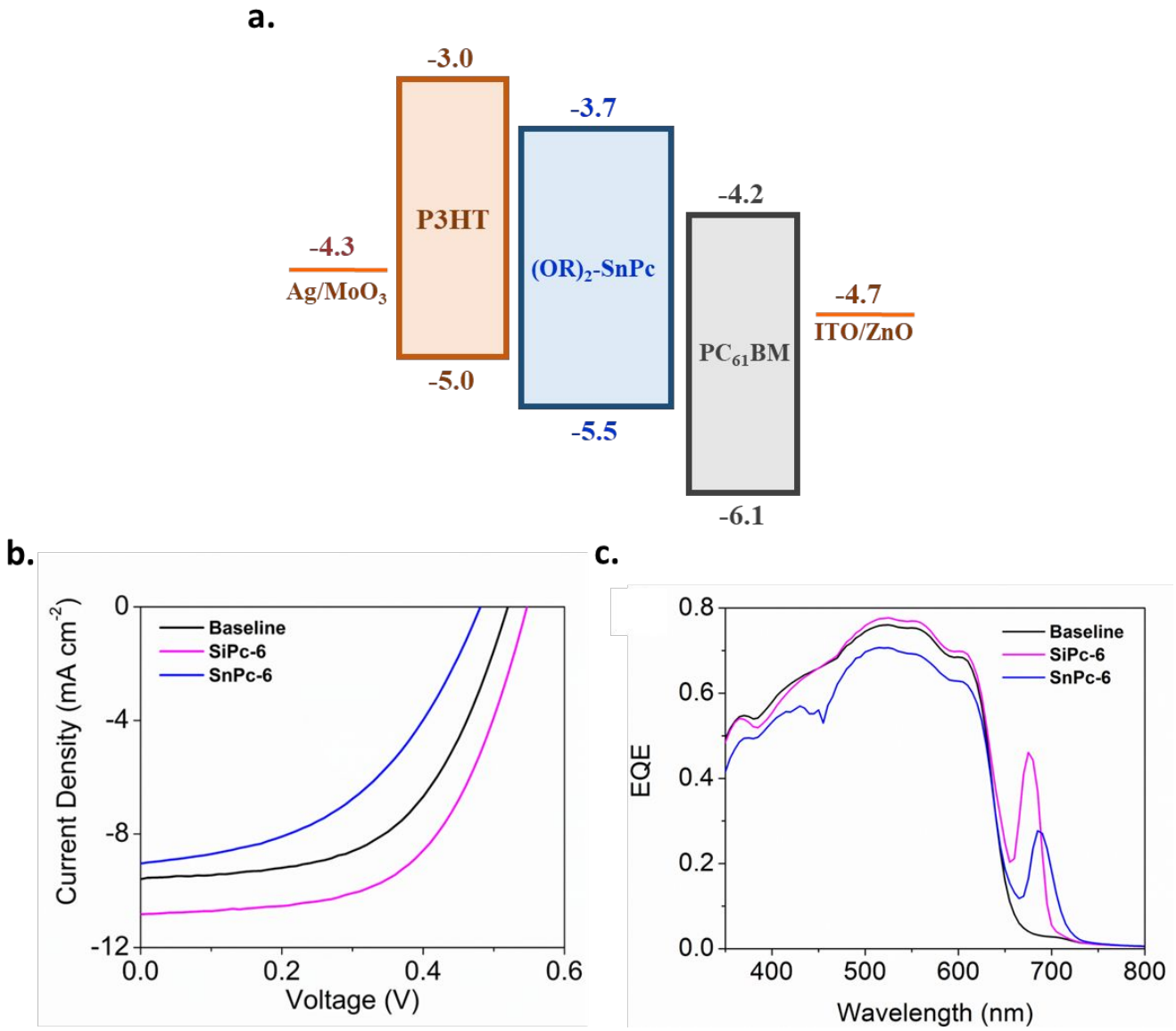

Figure 3. (a) OPV device structure and energy levels, (b) comparison between I-V curves, and (c) EQE curves of ternary OPV devices containing **SnPc-6** or the analogous **SiPc-6** additive[30] and P3HT/$PC_{61}BM$ baseline (no additive).

Organic thin-film transistors (OTFTs)

OTFTs were fabricated using **SnPc-1**, **SnPc-2**, **SnPc-4**, **SnPc-5**, **SnPc-6** and **SnPc-7** (**Figure 2**) as the semiconductor. Device characterization was performed at room temperature in a controlled nitrogen environment to determine μ_e (**Equation 4**), V_T, and $I_{on/off}$. **Figure 4** depicts example transfer curves for all characterized materials for annealed devices, with forward and reverse transfer curves displayed in **Figure S10** and output curves displayed in **Figure S11**.

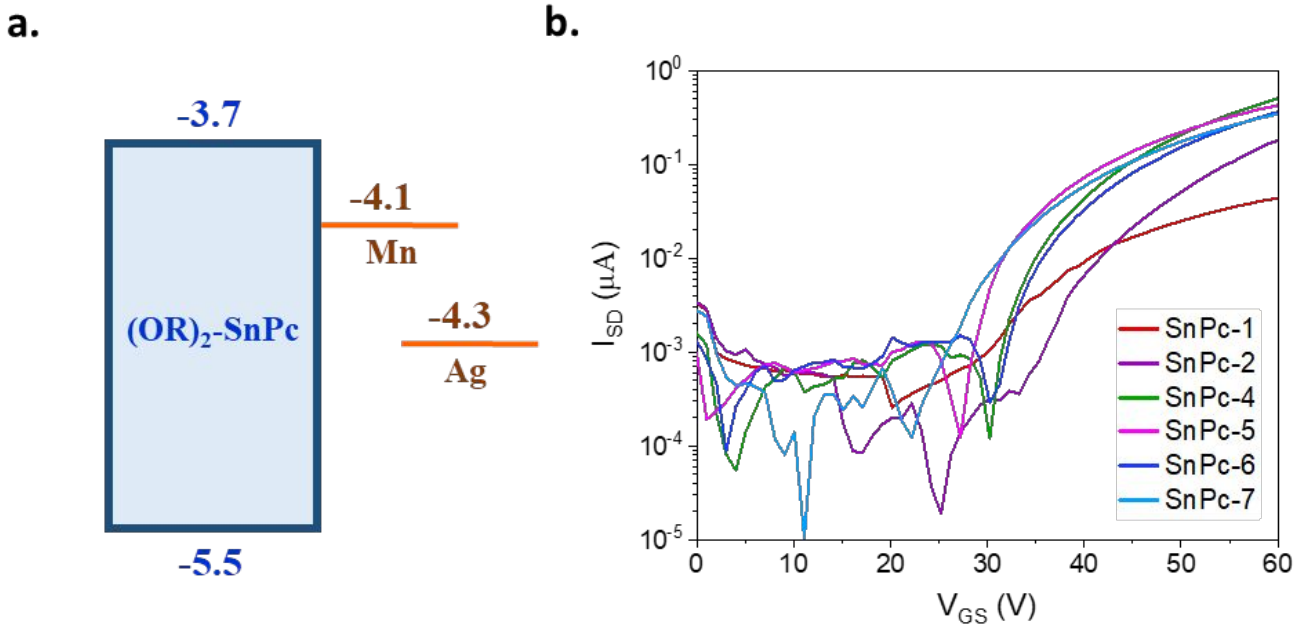

Figure 4. (a) Structure and energy levels of the semiconductors and electrodes,[60] and (b) example transfer curves of all $(OR)_2$-SnPc transistors characterized at room temperature in nitrogen. $(OR)_2$-SnPc films were spun from chloroform at 1500 RPM for 90 s and annealed at 100˚C for 1 h.

Table 5 summarizes the electrical characteristics of OTFTs with non-annealed and annealed thin-films. Annealing the $(OR)_2$-SnPc films at 100˚C had no significant effect on OTFT performance, with μ_e and V_T differences remaining within the calculated standard deviation of each material. Annealed films of **SnPc-4**, **SnPc-5**, **SnPc-6**, and **SnPc-7** all displayed similar semiconducting characteristics with small variations in μ_e, V_T in the range of 24.6 – 31.4 V, and an $I_{on/off}$ of 10^4. Material **SnPc-4** exhibited the highest maximum μ_e of 1.40 x 10^{-2} cm^2 V^{-1} s^{-1} with an average μ_e of 4.66 x 10^{-3} cm^2 V^{-1} s^{-1} for annealed films, but also a relatively high V_T of 31.4 V. Of the six $(OR)_2$-SnPcs investigated in devices, materials **SnPc-1** and **SnPc-2** resulted in the worst electrical performances in OTFTs, with **SnPc-1** having the lowest maximum and average μ_e for both annealed and non-annealed devices. Although **SnPc-2** displayed average μ_e comparable to the other $(OR)_2$-SnPcs (1.46 x 10^{-3} cm^2 V^{-1} s^{-1}), **2** exhibited the highest V_T of 52.6 V with very low $I_{on/off}$. The high V_T of these OTFTs is likely a cause of high contact resistance potentially due to a number of factors including the difference between the LUMO of the $(OR)_2$-SnPcs and the work function of the source-drain electrodes, the creation of interfacial dipoles, and

the presence of charge traps at the $(OR)_2$-SnPc-electrode interface.[13] A number of strategies are available to reduce the contact resistance of OTFTs by lowering the injection barrier through contact interlayer and electrode material engineering.[13] However, to demonstrate a comparison between SiPc based OTFT devices and SnPc based OTFT devices identical device configuration and processing conditions must be used. Finally, the axial groups on the phthalocyanines play a role on the V_T of devices, increasing the electron-withdrawing character of the axial pendant groups leads to a drop in V_T.[61]

Table 5. Summary of BGTC $(OR)_2$-SnPc and $(OR)_2$-SiPc transistor characteristics, measured at room temperature in a nitrogen atmosphere. Averages were calculated from forty unique transistors.

$(OR)_2$-SnPc Data					
Material	**Annealing Temp (˚C)**	**$\mu_{e,\,max}$[a] (x 10^{-2} cm^2 V^{-1} s^{-1})**	**$\mu_{e,\,avg}$[b] (x 10^{-2} cm^2 V^{-1} s^{-1})**	**V_T[c] (V)**	**$I_{on/off}$[d]**
SnPc-1	25	0.05438	0.0383 ± 0.010	26.8 ± 3.3	10^3
	100	0.0187	0.0153 ± 0.0014	21.7 ± 4.6	10^3
SnPc-2	25	0.246	0.174 ± 0.047	48.3 ± 3.8	10^0
	100	0.225	0.146 ± 0.035	52.6 ± 2.8	10^0
SnPc-4	25	1.14	0.245 ± 0.050	33.8 ± 1.2	10^4
	100	1.40	0.466 ± 0.23	31.4 ± 0.85	10^4
SnPc-5	25	0.924	0.407 ± 0.041	26.4 ± 3.6	10^4
	100	0.340	0.200 ± 0.068	24.6 ± 6.5	10^4
SnPc-6	25	0.819	0.208 ± 0.028	27.6 ± 4.4	10^4
	100	0.393	0.300 ± 0.089	27.2 ± 7.6	10^4
SnPc-7	25	1.09	0.716 ± 0.14	31.9 ± 2.9	10^2
	100	0.248	0.156 ± 0.049	25.6 ± 5.8	10^4
$(OR)_2$-SiPc Data[e]					
Material	**Annealing Temp (˚C)**	**$\mu_{e,\,max}$[a] (x 10^{-2} cm^2 V^{-1} s^{-1})**	**$\mu_{e,\,avg}$[b] (x 10^{-2} cm^2 V^{-1} s^{-1})**	**V_T[c] (V)**	**$I_{on/off}$[d]**
SiPc-1	25	0.208	0.137 ± 0.044	27.3 ± 1.6	10^4
	100	0.247	0.175 ± 0.025	24.9 ± 2.0	10^3
SiPc-2	25	0.0322	0.0171 ± 0.0079	43.1 ± 1.2	10^2
	100	0.0321	0.0151 ± 0.014	42.4 ± 9.4	10^3
SiPc-4	25	0.141	0.0820 ± 0.021	22.8 ± 2.4	10^4
	100	0.202	0.163 ± 0.023	16.8 ± 2.4	10^4
SiPc-5	25	0.888	0.734 ± 0.094	32.6 ± 3.5	10^5
	100	4.34	2.80 ± 0.53	17.6 ± 2.3	10^5
SiPc-6	25	-[f]	-[f]	-[f]	-[f]
	100	-[f]	-[f]	-[f]	-[f]
SiPc-7	25	0.0405	0.0284 ± 0.0091	39.1 ± 0.8	10^3
	100	0.0356	0.0111 ± 0.0023	30.6 ± 8.2	10^3

a. maximum saturation regime electron field-effect mobility ($\mu_{e,\,max}$)
b. mean saturation regime electron field-effect mobility ($\mu_{e,\,avg}$)
c. mean threshold voltage (V_T)
d. on/off current ratio ($I_{on/off}$)
e. data from ref [44]
f. non-functional device

Comparison of the DFT-calculated mobilities (**Table 3**) with experimentally found average μ_e in **Table 5** shows, in general, similar trends. DFT modeling predicted that materials **SnPc-5**, **SnPc-6** and **SnPc-7** would have similar μ_e values, and material **SnPc-1** was predicted to have the lowest μ_e value, all of which was observed experimentally. The biggest discrepancy was observed for material **SnPc-2**, which was predicted to have the largest mobility but instead resulted in devices with the second lowest performance.

In a previous report, the effect of axial substituents shown in **Figure 2** were studied using $(OR)_2$-SiPcs with identical axial groups, and characterized in OTFTs using the same fabrication conditions and architecture as the current study (**Table 5**).[44] Four of the six SnPcs (**SnPc-2**, **SnPc-4**, **SnPc-6**, and **SnPc-7**) displayed higher μ_e with similar V_T values compared to their $(OR)_2$-SiPc counterparts (**SiPc-2**, **SiPc-4**, **SiPc-6**, and **SiPc-7**);[44] **SnPc-5** and **SnPc-6** have higher μ_e and lower V_T compared to **SiPc-5** and **SiPc-6**, respectively, which were characterized in bottom-gate bottom-contact (BGBC) OTFTs.[26] **SnPc-1** and **SnPc-5** performed significantly better than **SiPc-1** and **SiPc-5** analogs, with maximum and average μ_e that are two orders of magnitude higher while maintaining similar V_T values.[44] Moreover, it is possible to reduce V_T and increase $I_{on/off}$ by further optimizing processing conditions and choice of axial groups.[61] These encouraging results suggest that, in OTFTs, $(OR)_2$-SnPcs can outperform $(OR)_2$-SiPc derivatives, further justifying their investigation.

AFM was performed to compare the thin-film morphology of the $(OR)_2$-SnPcs derivatives, and to correlate their thin-film microstructure to OTFT performance (**Figure 5**). **SnPc-2**, **SnPc-6**, and **SnPc-7** exhibited larger crystal-like features compared to **SiPc-2**, **SiPc-6**, and **SiPc-7**,[44] potentially contributing to the higher μ_e observed in these OTFTs due to increased grain interconnectivity, promoting more efficient charge transfer.[59,62] In contrast, **SnPc-4**, which exhibited the greatest μ_e of 1.40 x 10^{-2} cm^2 V^{-1} s^{-1}, displayed smaller and denser spherical grains. The low surface roughness, indicating a more homogenous thin-film formed by **SnPc-4** (**Figure 5**), contributed to the improved device performance.

Thin-films of **SnPc-1** have significantly larger features, with many distinct grain boundaries, and higher surface roughness compared to the other five materials. Large grain boundaries and height differences within the thin-film have been shown to reduce charge carrier μ_e and result in worse electrical performance in OTFTs.[57–59] Through XRD, the distance between crystal planes was determined by **Equation 6** to be between 10.0 – 13.8 Å for the $(OR)_2$-SnPcs (**Figure S8**), corroborating the lack of correlation between OTFT performance and thin-film microstructure. Furthermore, the lack of absolute correlation between electron mobility values computed in crystals and measured in thin-films also suggests that charge transport efficiency in this series of materials is mostly driven by thin-film morphology effects, rather than crystal structure.

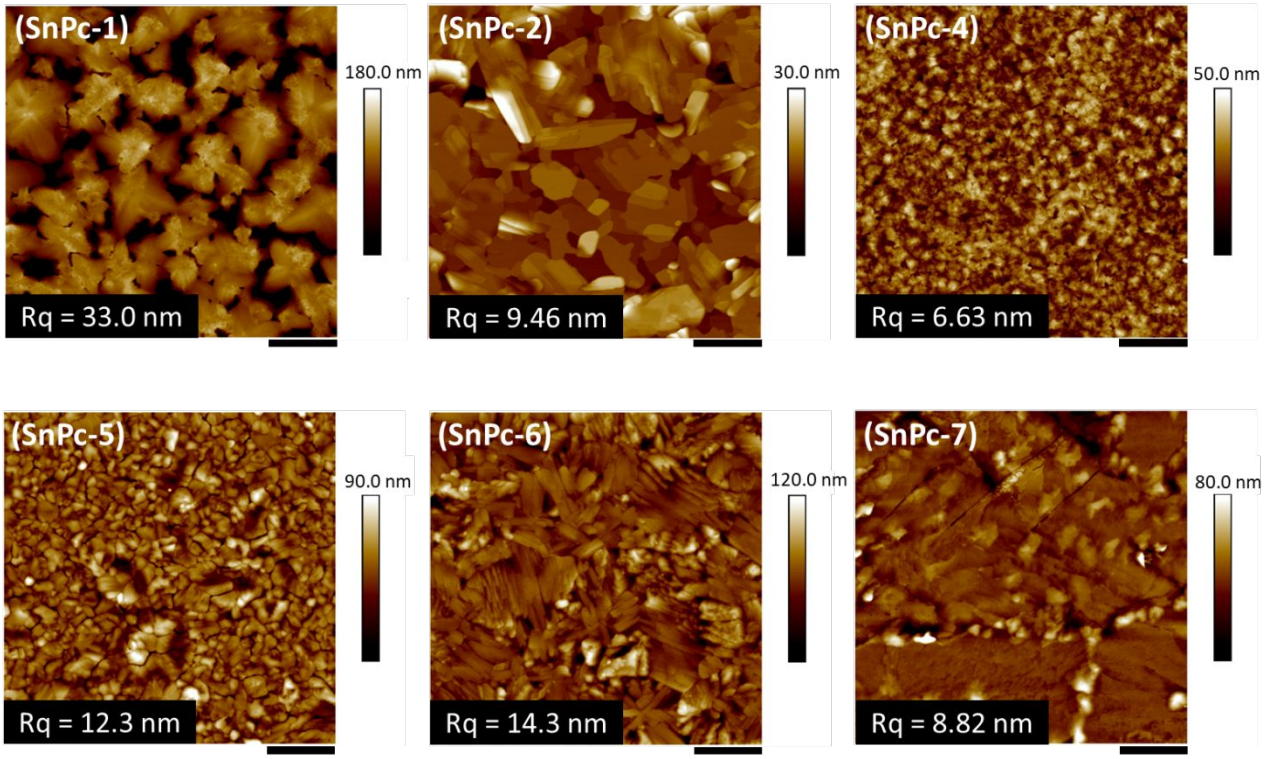

Figure 5. AFM images (10 µm x 10 µm) of $(OR)_2$-SnPc thin-films in OTFT devices. Black scale bar represents 2.0 µm. All films were spun from chloroform at 1500 RPM for 90 s and annealed at 100˚C for 1 h.

To further examine differences in electrical performance between $(OR)_2$-SnPcs, the interface charge trap density (N_i) was estimated using the subthreshold region of the characteristic transfer curves

displayed in **Figure 4** using **Equation 5**.[53,54] **Table S2** reports the estimated N_i for annealed devices of each characterized material, ranging from 1.96 x 10^{12} – 1.98 x 10^{13} cm^{-2} V^{-1}. The trap densities between the $(OR)_2$-SnPc materials and the reported value of 6.4 x 10^{12} cm^{-2} V^{-1} for vapour deposited copper phthalocyanine (CuPc) on OTS treated SiO_2[63] are comparable. Given the similarity in trap densities between the $(OR)_2$-SnPcs and CuPc, the differences in observed performance can be attributed to material characteristics, film formation, and microstructure rather than wafer properties.

Photostability of SnPcs

To investigate the contrasting performance of our SnPc derivatives compared to SiPcs in OPV and OTFT devices, the photostability of both the $(OR)_2$-SnPcs and $(OR)_2$-SiPc derivatives was assessed by measuring OTFT performance under AM1.5 solar simulator illumination using **SnPc-5** and **SiPc-5** as example materials. The change in OTFT electrical performance with increasing exposure time to light is shown in **Figure 6** for these materials. The μ_e of devices prepared from **SnPc-5** decreased significantly from 4.58 x 10^{-3} cm^2 V^{-1} s^{-1} to 2.34 x 10^{-4} cm^2 V^{-1} s^{-1} after 45 min of light exposure, whereas unexposed baseline devices kept under ambient light exhibited little variation in performance (**Figure 6a**). Conversely, both exposed and unexposed **SiPc-5** devices showed little change in μ_e after illumination (**Figure 6b**). OTFTs prepared from both phthalocyanines exhibited more dramatic increases in V_T after light exposure, with an increase of 19.2 V for illuminated devices (9.2 V for baseline devices) for **SnPc-5**, and a slightly smaller increase of 12.2 V for illuminated (5.9 V for baseline) for **SiPc-5** devices. The decrease in μ_e and slightly larger increase in V_T observed in OTFTs prepared from **SnPc-5** indicate that the performance of $(OR)_2$-SnPc OTFTs deteriorates with light exposure, which has little effect on $(OR)_2$-SiPc OTFTs. The temperature of the samples during these experiments never surpassed 25˚C (**Figure S12**), therefore the performance deterioration cannot be assigned to thermal degradation of the films. The poor shelf life of $(OR)_2$-SnPc as powders has also been observed. When rerunning NMR analysis for the samples after a few months (> 3 months), considerable degradation was observed. This degradation was

accelerated to < 12 hours when the derivatives were left in solution and when exposed to light (**Figure S18**), which is consistent with our device data.

The photostability of SnPcs has previously been studied by Nyokong *et al.* who showed that Cl_2-SnPcs can be photoreduced in the presence of electron donors (such as $SnCl_2$), forming a negatively charged $[Cl_2\text{-SnPc}]^{-1}$ molecule. The most likely mechanism is represented in **Scheme 1**, which involves the aggregation of SnPc excited states. The same group also showed that, when in solution, the photobleaching process happens in seconds upon light exposure.[55,64] Nyokong later was able to compare the photostability behaviour of different phthalocyanines and concluded that larger central atoms are associated with a greater susceptibility to photooxidation (due to the heavy atom effect).[64–66] This is in agreement with the different electrical performance we have observed for $(OR)_2$-SiPcs[30] and $(OR)_2$-SnPcs towards light exposure, and let us hypothesize this to be the chief reasoning for the poor OPV performance when using SnPcs as ternary additives.

$$Sn(IV)Pc \xrightarrow{hv} Sn(IV)Pc^{*}$$

$$2\,Sn(IV)Pc^{*} \rightarrow [Sn(IV)Pc^{*}]_2$$

$$[Sn(IV)Pc^{*}]_2 + R \xrightarrow{e^{-}\ exchange} 2\,Sn[(IV)Pc]^{-} + R^{2+}$$

Scheme 1. SnPc aggregation and bleaching mechanism proposed by Nyokong *et. al.*,[56] where *R* is a reducing species in contact with SnPc.

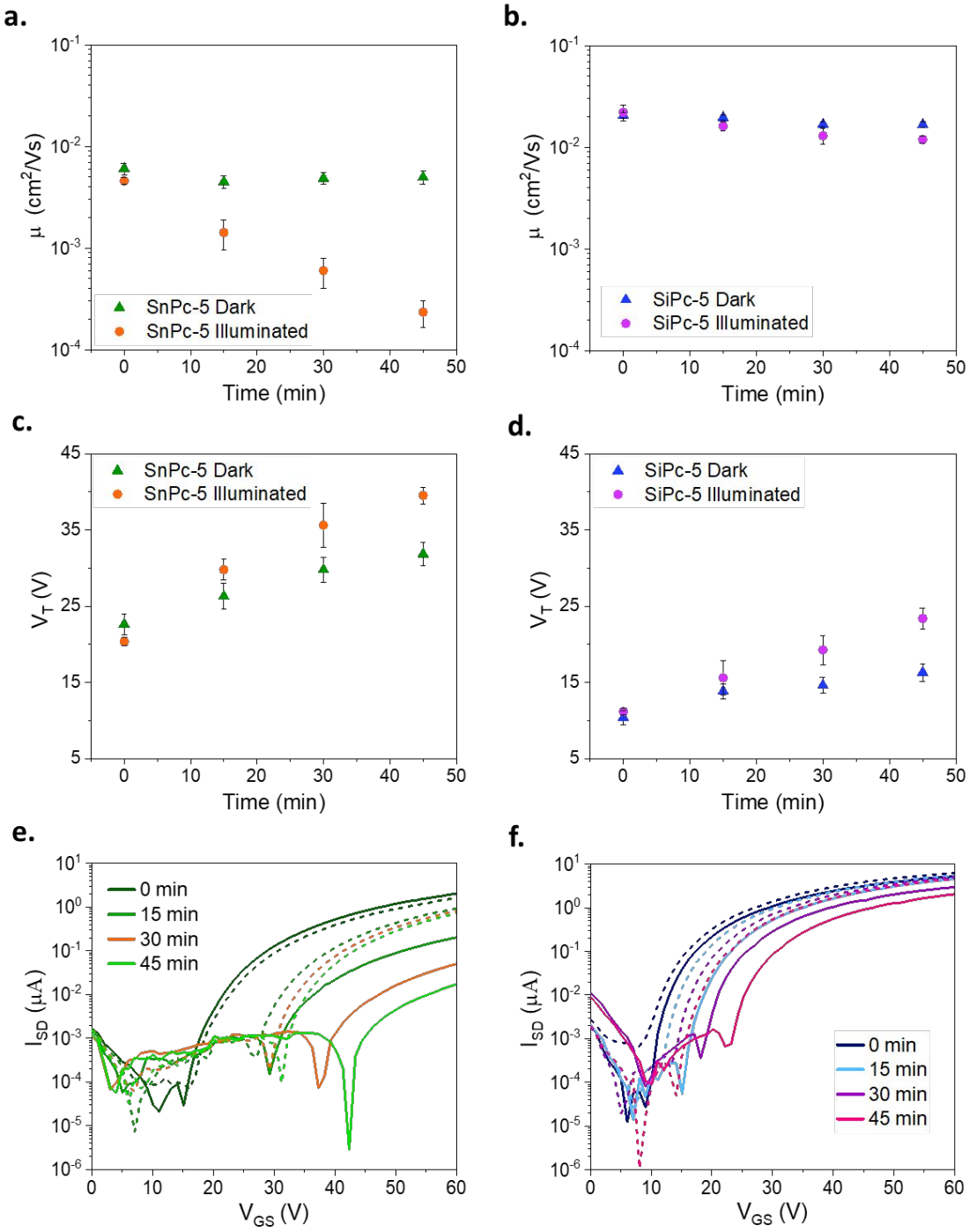

Figure 6. Change in μ_e and V_T for transistors prepared from (a, c) **SnPc-5** and (b, d) **SiPc-5**, and characteristic transfer curves of (e) **SnPc-5** and (f) **SiPc-5**. Transistors were characterized at room temperature in nitrogen after increasing exposure time to solar illumination, with dotted lines representing baseline devices with no light exposure. All films were spun from chloroform at 1500 RPM for 90 s and annealed at 100˚C for 1 h.

CONCLUSIONS

In this work six axially-substituted SnPcs, including four novel compounds, were successfully synthesized and characterized with respect to their structural, thermal, physical and opto-electronical properties; their applicability as ternary additives in OPVs and as active layers in solution processed OTFTs was also assessed. Incorporating the $(OR)_2$-SnPcs as additives in OPVs resulted in a reduction in device performance across all metrics when compared to the reference P3HT/$PC_{61}BM$ solar cell, the opposite of what was observed for their SiPcs counterparts. OTFTs fabricated with the $(OR)_2$-SnPcs exhibited average mobilities in the range of $0.02 – 0.70 \times 10^{-2}$ cm^2 V^{-1} s^{-1}, with four of the six compounds outperforming their SiPc counterparts in terms of mobility, while maintaining comparable threshold voltages in the range of 24 – 53 V. Through photostability characterization of OTFT devices, we have demonstrated that the poor OPV performance can be explained by the photodegradation of SnPcs. $(OR)_2$-SnPc OTFTs experienced a significant drop in their electrical performance after light exposure, which was not observed for analogous SiPc OTFTs. We conclusively show that while tetravalent SnPcs cannot be employed efficiently in applications that require light exposure, they outperform similar tetravalent phthalocyanines in OTFTs.

ASSOCIATED CONTENT

Supporting Information

The Supporting Information file is available free of charge.

crystal structures of materials determined by single crystal X-ray diffraction; UV-vis spectra of novel $(OR)_2$-SnPcs, CV spectra of novel $(OR)_2$-SnPcs, TGA thermal curves of novel $(OR)_2$-SnPcs, DSC thermograms of novel $(OR)_2$-SnPcs, non-negligible electron transfer integrals calculated between a reference molecule and its first neighbours; XRD patterns of **SnPc-4** polymorphs predicted from single crystal and measured from thin-films, C-N bond lengths within the conjugated backbone of **SnPc-1** and **SnPc-7,** XRD pattern of functional materials measured from thin-films, example transfer curves of

$(OR)_2$-SnPc transistors characterized at room temperature, forward and reverse transfer curves, characteristic output curves, interfacial charge trap density (N_i) of materials calculated from thin-films, plot of device temperature with increasing exposure time to solar illumination, ^{1}H NMR and ^{13}C NMR spectra of $(OR)_2$-SnPcs, ^{1}H NMR spectrum of **SnPc-4** after 12 h of exposure to ambient light.

Author Information

Corresponding Author

*Benoît H. Lessard - University of Ottawa, Department of Chemical and Biological Engineering, 161 Louis Pasteur, Ottawa, ON, Canada, K1N 6N5. Email: benoit.lessard@uottawa.ca

Author Contributions

The manuscript was written through contributions of all authors. All authors have given approval to the final version of the manuscript. R.R.C. and M.C.V conducted the experimental work, data analysis and wrote the initial draft of the manuscript. F.C., C.T and L.M. conducted DFT calculations with analysis, and assisted in writing and editing of the manuscript. N.A.R conducted AFM imaging and analysis and assisted in editing the manuscript. J.B., and B.H.L., acquired funding, managed supervision, directed the study as well as assisted in editing the manuscript.

Funding Sources

The Natural Sciences and Engineering Research Council of Canada (NSERC, RGPIN/2015-509 03987 and STPGP 506661-17 to B.H.L) and the University of Ottawa are acknowledged for financial support. The research was undertaken, in part, thanks to funding from the Canada Research Chair program which B.H.L is a member.

Acknowledgments

Computer time was provided by the Mésocentre de Calcul Intensif Aquitain (MCIA) of the University of Bordeaux and financed by the Conseil Régional d'Aquitaine and the French Ministry of Research and Technology. We also thank the Centre for Research in Photonics at the University of Ottawa (CRPuO) for access to the AFM and Dr. Ovens for performing single crystal X-ray diffraction.

REFERENCES

(1) Claessens, C. G.; Hahn, U.; Torres, T. Phthalocyanines: From Outstanding Electronic Properties to Emerging Applications. *Chem. Rec.* **2008**, *8* (2), 75–97. https://doi.org/10.1002/tcr.20139.

(2) A. Melville, O.; H. Lessard, B.; P. Bender, T. Phthalocyanine-Based Organic Thin-Film Transistors: A Review of Recent Advances. *ACS Appl. Mater. & Interfaces* **2015**, *7* (24), 13105–13118. https://doi.org/10.1021/acsami.5b01718.

(3) Boileau, N. T.; Cranston, R.; Mirka, B.; Melville, O. A.; Lessard, B. H. Metal Phthalocyanine Organic Thin-Film Transistors: Changes in Electrical Performance and Stability in Response to Temperature and Environment. *RSC Adv.* **2019**, *9* (37), 21478–21485. https://doi.org/10.1039/c9ra03648b.

(4) Lessard, B. H.; White, R. T.; Al-Amar, M.; Plint, T.; Castrucci, J. S.; Josey, D. S.; Lu, Z. H.; Bender, T. P. Assessing the Potential Roles of Silicon and Germanium Phthalocyanines in Planar Heterojunction Organic Photovoltaic Devices and How Pentafluoro Phenoxylation Can Enhance π-π Interactions and Device Performance. *ACS Appl. Mater. Interfaces* **2015**, *7* (9), 5076–5088. https://doi.org/10.1021/am508491v.

(5) Yuen, A. P.; Jovanovic, S. M.; Hor, A. M.; Klenkler, R. A.; Devenyi, G. A.; Loutfy, R. O.; Preston, J. S. Photovoltaic Properties of M-Phthalocyanine/Fullerene Organic Solar Cells. *Sol. Energy* **2012**, *86* (6), 1683–1688. https://doi.org/10.1016/j.solener.2012.03.019.

(6) Dang, M.-T.; Grant, T. M.; Yan, H.; Seferos, D. S.; Lessard, B. H.; Bender, T. P.; Miller, J. a.; Goethem, E. M. Van; Kenney, M. E.; Lu, Z.-H. Bis(Tri-n-Alkylsilyl Oxide) Silicon Phthalocyanines: A Start to Establishing a Structure Property Relationship as Both Ternary Additives and Non-Fullerene Electron Acceptors in Bulk Heterojunction Organic Photovoltaic Devices. *J. Mater. Chem. A* **2017**, *126*, 3378–3379. https://doi.org/10.1039/C6TA10739G.

(7) Plint, T. G.; Lessard, B. H.; Bender, T. P. Doping Chloro Boron Subnaphthalocyanines and Chloro Boron Subphthalocyanine in Simple OLED Architectures Yields Warm White Incandescent-like Emissions. *Opt. Mater. (Amst).* **2018**, *75*, 710–718. https://doi.org/https://doi.org/10.1016/j.optmat.2017.11.028.

(8) Zysman-Colman, E.; S. Ghosh, S.; Xie, G.; Varghese, S.; Chowdhury, M.; Sharma, N.; B. Cordes,

D.; M. Z. Slawin, A.; D. W. Samuel, I. Solution-Processable Silicon Phthalocyanines in Electroluminescent and Photovoltaic Devices. *ACS Appl. Mater. & Interfaces* **2016**, *8* (14), 9247–9253. https://doi.org/10.1021/acsami.5b12408.

(9) Ke, L.; Gasparini, N.; Min, J.; Zhang, H.; Adam, M.; Rechberger, S.; Forberich, K.; Zhang, C.; Spiecker, E.; Tykwinski, R. R.; Brabec, C. J.; Ameri, T. Panchromatic Ternary/Quaternary Polymer/Fullerene BHJ Solar Cells Based on Novel Silicon Naphthalocyanine and Silicon Phthalocyanine Dye Sensitizers. *J. Mater. Chem. A* **2017**, *5* (6), 2550–2562. https://doi.org/10.1039/C6TA08729A.

(10) Grant, T. M.; Gorisse, T.; Dautel, O.; Wantz, G.; Lessard, B. H. Multifunctional Ternary Additive in Bulk Heterojunction OPV: Increased Device Performance and Stability. *J. Mater. Chem. A* **2017**, *5* (4), 1581–1587. https://doi.org/10.1039/c6ta08593h.

(11) Ke, L.; Min, J.; Adam, M.; Gasparini, N.; Hou, Y.; Perea, J. D.; Chen, W.; Zhang, H.; Fladischer, S.; Sale, A.-C.; Spiecker, E.; Tykwinski, R. R.; Brabec, C. J.; Ameri, T. A Series of Pyrene-Substituted Silicon Phthalocyanines as Near-IR Sensitizers in Organic Ternary Solar Cells. *Adv. Energy Mater.* **2016**, *6* (7), 1502355. https://doi.org/10.1002/aenm.201502355.

(12) Faure, M. D. M.; Grant, T. M.; Lessard, B. H. Silicon Phthalocyanines as Acceptor Candidates in Mixed Solution/Evaporation Processed Planar Heterojunction Organic Photovoltaic Devices. *Coatings* **2019**, *9* (3). https://doi.org/10.3390/COATINGS9030203.

(13) Melville, O. A.; Grant, T. M.; Lochhead, K.; King, B.; Ambrose, R.; Rice, N. A.; Boileau, N. T.; Peltekoff, A. J.; Tousignant, M.; Hill, I. G.; Lessard, B. H. Contact Engineering Using Manganese, Chromium, and Bathocuproine in Group 14 Phthalocyanine Organic Thin-Film Transistors. *ACS Appl. Electron. Mater.* **2020**, *2* (5), 1313–1322. https://doi.org/10.1021/acsaelm.0c00104.

(14) Melville, O. A.; Grant, T. M.; Lessard, B. H. Silicon Phthalocyanines as N-Type Semiconductors in Organic Thin Film Transistors. *J. Mater. Chem. C* **2018**, *6* (20), 5482–5488. https://doi.org/10.1039/c8tc01116h.

(15) Bonardi, A.-H.; Bonardi, F.; Morlet-Savary, F.; Dietlin, C.; Noirbent, G.; M. Grant, T.; Fouassier, J.-P.; Dumur, F.; H. Lessard, B.; Gigmes, D.; Lalevée, J. Photoinduced Thermal Polymerization Reactions. *Macromolecules* **2018**, *51* (21), 8808–8820.

https://doi.org/10.1021/acs.macromol.8b01741.

(16) H. Bonardi, A.; Dumur, F.; M. Grant, T.; Noirbent, G.; Gigmes, D.; H. Lessard, B.; Fouassier, J.-P.; Lalevée, J. High Performance Near-Infrared (NIR) Photoinitiating Systems Operating under Low Light Intensity and in the Presence of Oxygen. *Macromolecules* **2018**, *51* (4), 1314–1324. https://doi.org/10.1021/acs.macromol.8b00051.

(17) Li, K.; Qiu, L.; Liu, Q.; Lv, G.; Zhao, X.; Wang, S.; Lin, J. Conjugate of Biotin with Silicon(IV) Phthalocyanine for Tumor-Targeting Photodynamic Therapy. *J. Photochem. Photobiol. B Biol.* **2017**, *174* (August), 243–250. https://doi.org/10.1016/j.jphotobiol.2017.08.003.

(18) Mitra, K.; Samsó, M.; Lyons, C. E.; Hartman, M. C. T. Hyaluronic Acid Grafted Nanoparticles of a Platinum(Ii)-Silicon(Iv) Phthalocyanine Conjugate for Tumor and Mitochondria-Targeted Photodynamic Therapy in Red Light. *J. Mater. Chem. B* **2018**, *6* (45), 7373–7377. https://doi.org/10.1039/C8TB02533A.

(19) Zhang, Y.; Lovell, J. F. Recent Applications of Phthalocyanines and Naphthalocyanines for Imaging and Therapy. *Wiley Interdisciplinary Reviews: Nanomedicine and Nanobiotechnology*. 2017. https://doi.org/10.1002/wnan.1420.

(20) Yutronkie, N. J.; Grant, T. M.; Melville, O. A.; Lessard, B. H.; Brusso, J. L. Old Molecule, New Chemistry: Exploring Silicon Phthalocyanines as Emerging N-Type Materials in Organic Electronics. *Materials (Basel)*. **2019**, *12* (8), 5–10. https://doi.org/10.3390/ma12081334.

(21) Kim, D. Y.; Sarasqueta, G.; So, F. SnPc:C60 Bulk Heterojunction Organic Photovoltaic Cells with MoO3 Interlayer. *Sol. Energy Mater. Sol. Cells* **2009**, *93* (8), 1452–1456. https://doi.org/10.1016/j.solmat.2009.03.011.

(22) Lin, W. K.; Su, S. H.; Ma, C. K.; Yokoyama, M. Enhancing Conversion Efficiency of Inverted Organic Solar Cells Using Ag Nanoparticles and Long Wavelength Absorbing Tin (II) Phthalocyanine. *Org. Electron.* **2016**, *29*, 94–98. https://doi.org/10.1016/j.orgel.2015.11.030.

(23) Rand, B. P.; Xue, J.; Yang, F.; Forrest, S. R. Organic Solar Cells with Sensitivity Extending into the near Infrared. *Appl. Phys. Lett.* **2005**, *87* (23), 1–3. https://doi.org/10.1063/1.2140075.

(24) Lai, H.; Li, X.; Li, S.; Chen, Y.; Sun, B.; Jiang, Q.; Yang, J. Enhancement of Photovoltaic

Performance and Moisture Stability of Perovskite Solar Cells by Modification of Tin Phthalocyanine (SnPc). *Electrochim. Acta* **2019**, *296*, 799–805. https://doi.org/10.1016/j.electacta.2018.10.087.

(25) Sharma, G. D.; BalaRaju, P.; Roy, M. S. Effect of Functional Groups of Acceptor Material on Photovoltaic Response of Bulk Hetero-Junction Organic Devices Based on Tin Phthalocyanine (SnPc). *Sol. Energy Mater. Sol. Cells* **2008**, *92* (3), 261–272. https://doi.org/10.1016/j.solmat.2007.08.013.

(26) Grant, T. M.; A. Rice, N.; Muccioli, L.; Castet, F.; H. Lessard, B. Solution-Processable n-Type Tin Phthalocyanines in Organic Thin Film Transistors and as Ternary Additives in Organic Photovoltaics. *ACS Appl. Electron. Mater.* **2019**, *1* (4), 494–504. https://doi.org/10.1021/acsaelm.8b00113.

(27) Honda, S.; Nogami, T.; Ohkita, H.; Benten, H.; Ito, S. Improvement of the Light-Harvesting Efficiency in Polymer/Fullerene Bulk Heterojunction Solar Cells by Interfacial Dye Modification. *ACS Appl. Mater. Interfaces* **2009**, *1* (4), 804–810. https://doi.org/10.1021/am800229p.

(28) Honda, S.; Ohkita, H.; Benten, H.; Ito, S. Selective Dye Loading at the Heterojunction in Polymer/Fullerene Solar Cells. *Adv. Energy Mater.* **2011**, *1* (4), 588–598. https://doi.org/10.1002/aenm.201100094.

(29) Honda, S.; Yokoya, S.; Ohkita, H.; Benten, H.; Ito, S. Light-Harvesting Mechanism in Polymer/Fullerene/Dye Ternary Blends Studied by Transient Absorption Spectroscopy. *J. Phys. Chem. C* **2011**, *115* (22), 11306–11317. https://doi.org/10.1021/jp201742v.

(30) Vebber, M. C.; Grant, T. M.; Brusso, J. L.; Lessard, B. H. Bis(Trialkylsilyl Oxide) Silicon Phthalocyanines: Understanding the Role of Solubility in Device Performance as Ternary Additives in Organic Photovoltaics. *Langmuir* **2020**, *36* (10), 2612–2621. https://doi.org/10.1021/acs.langmuir.9b03772.

(31) Someya, T.; Sekitani, T.; Iba, S.; Kato, Y.; Kawaguchi, H.; Sakurai, T. A Large-Area, Flexible Pressure Sensor Matrix with Organic Field-Effect Transistors for Artificial Skin Applications. *Proc. Natl. Acad. Sci. U. S. A.* **2004**, *101* (27), 9966–9970. https://doi.org/10.1073/pnas.0401918101.

(32) Gelinck, G. H.; Huitema, H. E. A.; Veenendaal, E. Van; Cantatore, E.; Schrijnemakers, L.; Van Der Putten, J. B. P. H.; Geuns, T. C. T.; Beenhakkers, M.; Giesbers, J. B.; Huisman, B. H.; Meijer, E. J.; Benito, E. M.; Touwslager, F. J.; Marsman, A. W.; Van Rens, B. J. E.; De Leeuw, D. M. Flexible Active-Matrix Displays and Shift Registers Based on Solution-Processed Organic Transistors. *Nat. Mater.* **2004**, *3* (2), 106–110. https://doi.org/10.1038/nmat1061.

(33) Zhou, L.; Wanga, A.; Wu, S. C.; Sun, J.; Park, S.; Jackson, T. N. All-Organic Active Matrix Flexible Display. *Appl. Phys. Lett.* **2006**, *88* (8), 2004–2007. https://doi.org/10.1063/1.2178213.

(34) Kumar, B.; Kaushik, B. K.; Negi, Y. S. Organic Thin Film Transistors: Structures, Models, Materials, Fabrication, and Applications: A Review. *Polym. Rev.* **2014**, *54* (1), 33–111. https://doi.org/10.1080/15583724.2013.848455.

(35) Song, D.; Zhu, F.; Yu, B.; Huang, L.; Geng, Y.; Yan, D. Tin (IV) Phthalocyanine Oxide: An Air-Stable Semiconductor with High Electron Mobility. *Appl. Phys. Lett.* **2008**, *92* (14), 2–5. https://doi.org/10.1063/1.2903486.

(36) Song, D.; Wang, H.; Zhu, F.; Yang, J.; Tian, H.; Geng, Y.; Yan, D. Phthalocyanato Tin(IV) Dichloride: An Air-Stable, High-Performance, n-Type Organic Semiconductor with a High Field-Effect Electron Mobility. *Adv. Mater.* **2008**, *20* (11), 2142–2144. https://doi.org/10.1002/adma.200702439.

(37) Bao, B. Z.; Lovinger, A. J.; Dodabalapur, A. Highly Ordered Vacuum-Deposited Thin Films of Metallophthalocyanines and Their Applications in Field-Effect Transistors. *Adv. Mater.* **1997**, *9* (1), 42–44.

(38) Sung, A.; Ling, M. M.; Tang, M. L.; Bao, Z.; Locklin, J. Correlating Molecular Structure to Field-Effect Mobility: The Investigation of Side-Chain Functionality in Phenylene-Thiophene Oligomers and Their Application in Field Effect Transistors. *Chem. Mater.* **2007**, *19* (9), 2342–2351. https://doi.org/10.1021/cm070117n.

(39) Mei, J.; Kim, D. H.; Ayzner, A. L.; Toney, M. F.; Bao, Z. Siloxane-Terminated Solubilizing Side Chains: Bringing Conjugated Polymer Backbones Closer and Boosting Hole Mobilities in Thin-Film Transistors. *J. Am. Chem. Soc.* **2011**, *133* (50), 20130–20133. https://doi.org/10.1021/ja209328m.

(40) Osaka, I.; Zhang, R.; Sauvè, G.; Smilgies, D. M.; Kowalewski, T.; McCullough, R. D. High-Lamellar Ordering and Amorphous-like π-Network in Short-Chain Thiazolothiazole-Thiophene Copolymers Lead to High Mobilities. *J. Am. Chem. Soc.* **2009**, *131* (7), 2521–2529. https://doi.org/10.1021/ja801475h.

(41) Zhang, F.; Hu, Y.; Schuettfort, T.; Di, C.; Gao, X.; R. McNeill, C.; Thomsen, L.; C. B. Mannsfeld, S.; Yuan, W.; Sirringhaus, H.; Zhu, D. Critical Role of Alkyl Chain Branching of Organic Semiconductors in Enabling Solution-Processed N-Channel Organic Thin-Film Transistors with Mobility of up to 3.50 Cm2 V–1 s–1. *J. Am. Chem. Soc.* **2013**, *135* (6), 2338–2349. https://doi.org/10.1021/ja311469y.

(42) Zhang, C.; Zang, Y.; Zhang, F.; Diao, Y.; McNeill, C. R.; Di, C. an; Zhu, X.; Zhu, D. Pursuing High-Mobility n-Type Organic Semiconductors by Combination of "Molecule-Framework" and "Side-Chain" Engineering. *Adv. Mater.* **2016**, *28* (38), 8456–8462. https://doi.org/10.1002/adma.201602598.

(43) Gao, X.; Di, C.; Hu, Y.; Yang, X.; Fan, H.; Zhang, F.; Liu, Y.; Li, H.; Zhu, D. Core-Expanded Naphthalene Diimides Fused with 2-(1,3-Dithiol-2-Ylidene)Malonitrile Groups for High-Performance, Ambient-Stable, Solution-Processed n-Channel Organic Thin Film Transistors. *J. Am. Chem. Soc.* **2010**, *132* (11), 3697–3699. https://doi.org/10.1021/ja910667y.

(44) Cranston, R. R.; Vebber, M. C.; Berbigier, J. F.; Rice, N. A.; Tonnelé, C.; Comeau, Z. J.; Boileau, N. T.; Brusso, J. L.; Shuhendler, A. J.; Castet, F.; Muccioli, L.; Kelly, T. L.; Lessard, B. H. Thin-Film Engineering of Solution-Processable n-Type Silicon Phthalocyanines for Organic Thin-Film Transistors. *ACS Appl. Mater. Interfaces* **2021**, *13* (1), 1008–1020. https://doi.org/10.1021/acsami.0c17657.

(45) Lowbry, M. K.; Starshak, A. J.; John, S. J.; Esposito, N.; Krueger, P. C.; Kenney, M. E. Dichloro(Phthalocyanino)Silicon. *Inorg. Chem.* **1965**, *4* (1), 128. https://doi.org/10.1021/ic50023a036.

(46) Brédas, J. L.; Silbey, R.; Boudreaux, D. S.; Chance, R. R. Chain-Length Dependence of Electronic and Electrochemical Properties of Conjugated Systems: Polyacetylene, Polyphenylene, Polythiophene, and Polypyrrole. *J. Am. Chem. Soc.* **1983**, *105* (22), 6555–6559. https://doi.org/10.1021/ja00360a004.

(47) Manoj Gali, S.; Matta, M.; H. Lessard, B.; Castet, F.; Muccioli, L. Ambipolarity and Dimensionality of Charge Transport in Crystalline Group 14 Phthalocyanines: A Computational Study. *J. Phys. Chem. C* **2018**, *122* (5), 2554–2563. https://doi.org/10.1021/acs.jpcc.7b11588.

(48) Frisch, M. J.; Trucks, G. W.; Schlegel, H. B.; Scuseria, G. E.; Robb, M. A.; Cheeseman, J. R.; Scalmani, G.; Barone, V.; Petersson, G. A.; Nakatsuji, H.; Li, X.; Caricato, M.; Marenich, A. V.; Bloino, J.; Janesko, B. G.; Gomperts, R.; Mennucci, B.; Hratchian, H. P.; Ortiz, J. V.; Izmaylov, A. F.; Sonnenberg, J. L.; Williams-Young, D.; Ding, F.; Lipparini, F.; Egidi, F.; Goings, J.; Peng, B.; Petrone, A.; Henderson, T.; Ranasinghe, D.; Zakrzewski, V. G.; Gao, J.; Rega, N.; Zheng, G.; Liang, W.; Hada, M.; Ehara, M.; Toyota, K.; Fukuda, R.; Hasegawa, J.; Ishida, M.; Nakajima, T.; Honda, Y.; Kitao, O.; Nakai, H.; Vreven, T.; Throssell, K.; Montgomery, J. A., J.; Peralta, J. E.; Ogliaro, F.; Bearpark, M. J.; Heyd, J. J.; Brothers, E. N.; Kudin, K. N.; Staroverov, V. N.; Keith, T. A.; Kobayashi, R.; Normand, J.; Raghavachari, K.; Rendell, A. P.; Burant, J. C.; Iyengar, S. S.; Tomasi, J.; Cossi, M.; Millam, J. M.; Klene, M.; Adamo, C.; Cammi, R.; Ochterski, J. W.; Martin, R. L.; Morokuma, K.; Farkas, O.; Foresman, J. B.; Fox, D. J. Gaussian 16. Gaussian, Inc.: Wallingford CT 2016.

(49) Godbout, N.; Salahub, D. R.; Andzelm, J.; Wimmer, E. Optimization of Gaussian-Type Basis Sets for Local Spin Density Functional Calculations. Part I. Boron through Neon, Optimization Technique and Validation. *Can. J. Chem.* **1992**, *70* (2), 560–571. https://doi.org/10.1139/v92-079.

(50) Coropceanu, V.; Malagoli, M.; da Silva Filho, D. A.; Gruhn, N. E.; Bill, T. G.; Brédas, J. L. Hole- and Electron-Vibrational Couplings in Oligoacene Crystals: Intramolecular Contributions. *Phys. Rev. Lett.* **2002**, *89* (27), 1–4. https://doi.org/10.1103/PhysRevLett.89.275503.

(51) F. Valeev, E.; Coropceanu, V.; A. da Silva Filho, D.; Salman, S.; Brédas, J.-L. Effect of Electronic Polarization on Charge-Transport Parameters in Molecular Organic Semiconductors. *J. Am. Chem. Soc.* **2006**, *128* (30), 9882–9886. https://doi.org/10.1021/ja061827h.

(52) Neese, F. The ORCA Program System. *Wiley Interdiscip. Rev. Comput. Mol. Sci.* **2012**, *2* (1), 73–78. https://doi.org/10.1002/wcms.81.

(53) Kim, S. H.; Kang, I.; Kim, Y. G.; Hwang, H. R.; Kim, Y.-H.; Kwon, S.-K.; Jang, J. High Performance Ink-Jet Printed Diketopyrrolopyrrole-Based Copolymer Thin-Film Transistors Using a Solution-Processed Aluminium Oxide Dielectric on a Flexible Substrate. *J. Mater. Chem. C*

2013, *1* (13), 2408. https://doi.org/10.1039/c3tc00718a.

(54) Kalb, W. L.; Batlogg, B. Calculating the Trap Density of States in Organic Field-Effect Transistors from Experiment: A Comparison of Different Methods. *Phys. Rev. B - Condens. Matter Mater. Phys.* **2010**, *81* (3), 1–13. https://doi.org/10.1103/PhysRevB.81.035327.

(55) Nyokong, T. Photoreduction of Tin(IV) Phthalocyanines. *Polyhedron* **1994**, *13* (13), 2067–2071. https://doi.org/10.1016/S0277-5387(00)83491-9.

(56) Sakamoto, K.; Ohno-Okumura, E. Syntheses and Functional Properties of Phthalocyanines. *Materials (Basel).* **2009**, *2* (3), 1127–1179. https://doi.org/10.3390/ma2031127.

(57) Rivnay, J.; C. B. Mannsfeld, S.; E. Miller, C.; Salleo, A.; F. Toney, M. Quantitative Determination of Organic Semiconductor Microstructure from the Molecular to Device Scale. *Chem. Rev.* **2012**, *112* (10), 5488–5519. https://doi.org/10.1021/cr3001109.

(58) Chang, P. C.; Lee, J.; Huang, D.; Subramanian, V.; Murphy, A. R.; Fréchet, J. M. J. Film Morphology and Thin Film Transistor Performance of Solution-Processed Oligothiophenes. *Chem. Mater.* **2004**, *16* (23), 4783–4789. https://doi.org/10.1021/cm0496570.

(59) Oh, J. H.; Liu, S.; Bao, Z.; Schmidt, R.; Würthner, F. Air-Stable n -Channel Organic Thin-Film Transistors with High Field-Effect Mobility Based on N, N′ -Bis(Heptafluorobutyl)-3,4:9,10-Perylene Diimide. *Appl. Phys. Lett.* **2007**, *91* (21). https://doi.org/10.1063/1.2803073.

(60) Hölzl, J.; Schulte, F. K. *Work Function of Metals*; Springer: Berlin, 1979. https://doi.org/10.1007/bfb0048919.

(61) King, B.; Melville, O. A.; Rice, N. A.; Kashani, S.; Tonnelé, C.; Raboui, H.; Swaraj, S.; Grant, T. M.; McAfee, T.; Bender, T. P.; Ade, H.; Castet, F.; Muccioli, L.; Lessard, B. H. Silicon Phthalocyanines for N-Type Organic Thin-Film Transistors: Development of Structure−property Relationships. *ACS Appl. Electron. Mater.* **2021**. https://doi.org/10.1021/acsaelm.0c00871.

(62) Ling, M. M.; Erk, P.; Gomez, M.; Koenemann, M.; Locklin, J.; Bao, Z. Air-Stable n-Channel Organic Semiconductors Based on Perylene Diimide Derivatives without Strong Electron Withdrawing Groups. *Adv. Mater.* **2007**, *19* (8), 1123–1127. https://doi.org/10.1002/adma.200601705.

(63) Sinha, S.; Wang, C. H.; Mukherjee, M.; Yang, Y. W. The Effect of Gate Dielectric Modification and Film Deposition Temperature on the Field Effect Mobility of Copper (II) Phthalocyanine Thin-Film Transistors. *J. Phys. D. Appl. Phys.* **2014**, *47* (24). https://doi.org/10.1088/0022-3727/47/24/245103.

(64) Maree, S.; Phillips, D.; Nyokong, T. Synthesis, Photophysical and Photochemical Studies of Germanium and Tin Phthalocyanine Complexes. *J. Porphyr. Phthalocyanines* **2002**, *6* (1), 17–25. https://doi.org/10.1142/S108842460200004X.

(65) Nyokong, T. Effects of Substituents on the Photochemical and Photophysical Properties of Main Group Metal Phthalocyanines. *Coord. Chem. Rev.* **2007**, *251* (13-14 SPEC. ISS.), 1707–1722. https://doi.org/10.1016/j.ccr.2006.11.011.

(66) Nyokong, T. Electrocatalytic and Photosensitizing Behavior of Metallophthalocyanine Complexes. *J. Porphyr. Phthalocyanines* **2008**, *12* (9), 1005–1021. https://doi.org/10.1142/S1088424608000388.

FOR TABLE OF CONTENTS ONLY

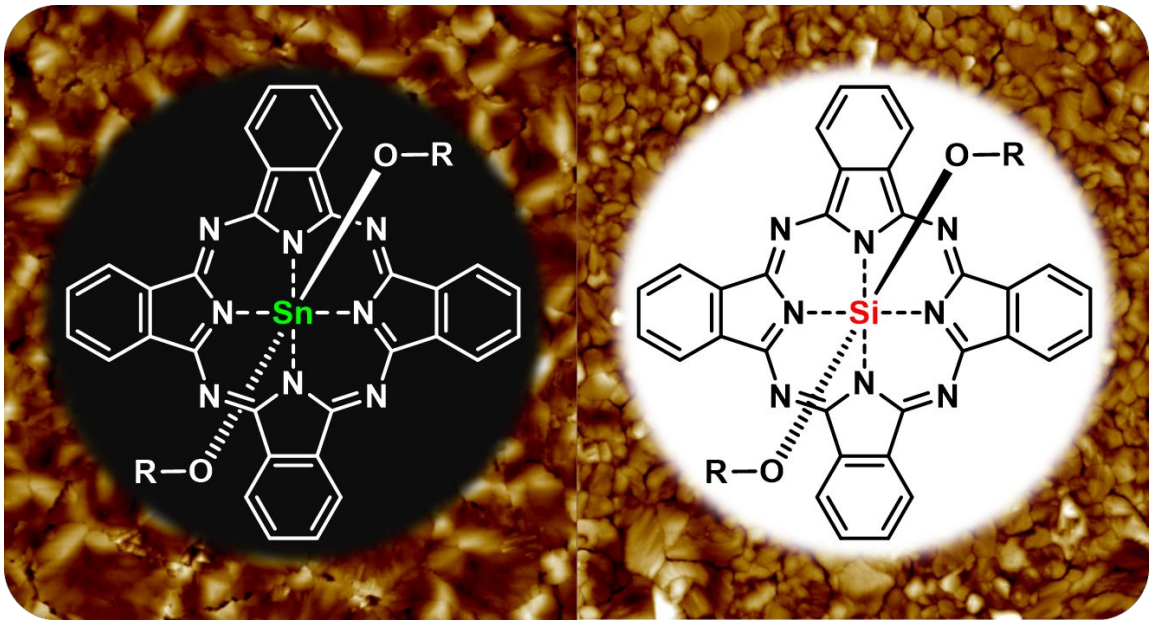

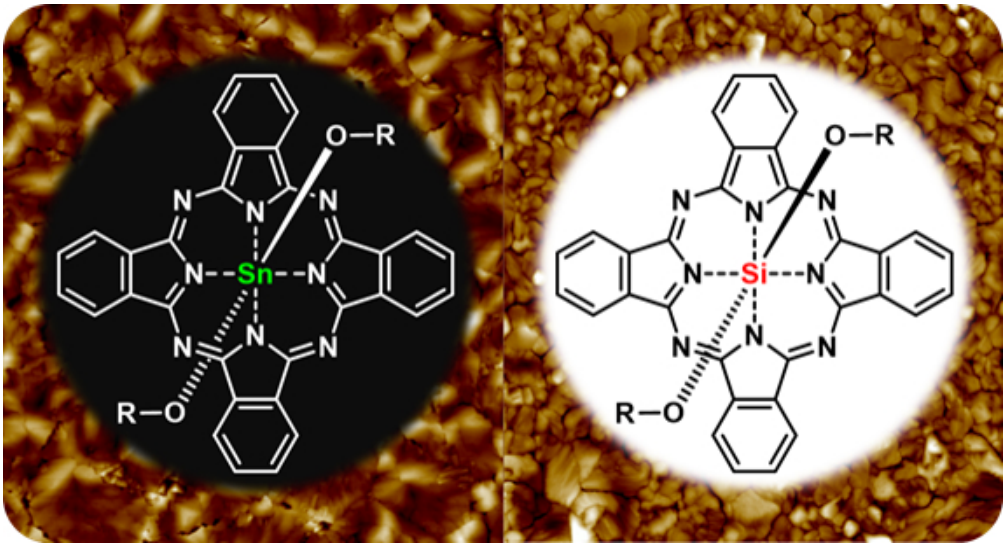

TOC

151x81mm (96 x 96 DPI)